Chemosphere 309 (2022) 136743

Contents lists available at ScienceDirect

Chemosphere

journal homepage: www.elsevier.com/locate/chemosphere

Elemental imaging approach to assess the ability of subaerial biofilms growing on constructions located in tropical climates as potential biomonitors of atmospheric heavy metals pollution

Euler Gallego-Cartagena [a,b,*], Héctor Morillas [c], Wendy Morgado-Gamero [d], Fabio Fuentes-Gandara [d], Víctor Vacca-Jimeno [e], Isabel Salcedo [f], Juan Manuel Madariaga [b], Maite Maguregui [g]

[a] Department of Civil and Environmental, Universidad de la Costa, Calle 58 #55-66, 080002, Barranquilla, Colombia
[b] Department of Analytical Chemistry, Faculty of Science and Technology, University of the Basque Country UPV/EHU, P.O. Box 644, 48080, Bilbao, Basque Country, Spain
[c] Department of Didactic of Mathematics, Experimental and Social Sciences, Faculty of Education and Sport, University of the Basque Country UPV/EHU, 01006, Vitoria-Gasteiz, Basque Country, Spain
[d] Department of Exact and Natural Sciences, Universidad de la Costa, Calle 58 #55-66, 080002, Barranquilla, Colombia
[e] Faculty of Basic Sciences, Universidad Del Atlántico, Km5 Vía Puerto Colombia, 081007, Atlántico, Colombia
[f] Department of Plant Biology and Ecology, Faculty of Science and Technology, University of the Basque Country UPV/EHU, P.O. Box 644, 48080, Bilbao, Basque Country, Spain
[g] Department of Analytical Chemistry, Faculty of Pharmacy, University of the Basque Country UPV/EHU, P.O. Box 450, 01080, Vitoria-Gasteiz, Basque Country, Spain

HIGHLIGHTS

- Subaerial biofilms (SABs) for passive biomonitoring studies of air quality in tropical cities.
- Deposition of metallic PM in SABs growing naturally on buildings from tropical cities.
- μ-EDXRF and SEM-EDS single point and imaging in SABs to assessment air pollution sources.
- Analytical methodologies for fast and cost-effective assessment of PM deposited in SABs.

GRAPHICAL ABSTRACT

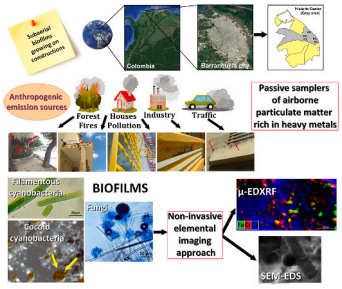

ARTICLE INFO

Handling Editor: Lena Q. Ma

Keywords:
Subaerial biofilms
Atmospheric heavy metals pollution
Construction materials
X-ray fluorescence imaging

ABSTRACT

Over the last decades, the concern about air pollution has increased significantly, especially in urban areas. Active sampling of air pollutants requires specific instrumentation not always available in all the laboratories. Passive sampling has a lower cost than active alternatives but still requires efforts to cover extensive areas. The use of biological systems as passive samplers might be a solution that provides information about air pollution to assist decision-makers in environmental health and urban planning. This study aims to employ subaerial biofilms (SABs) growing naturally on façades of historical and recent constructions as natural passive biomonitors of atmospheric heavy metals pollution. Concretely, SABs spontaneously growing on constructions located in a tropical climate, like the one of the city of Barranquilla (Colombia), have been used to develop the

* Corresponding author. Department of Civil and Environmental, Universidad de la Costa, Calle 58 #55-66, 080002, Barranquilla, Colombia.
E-mail addresses: egallego1@cuc.edu.co, egallego011@ikasle.ehu.eus (E. Gallego-Cartagena).

https://doi.org/10.1016/j.chemosphere.2022.136743
Received 25 July 2022; Received in revised form 30 September 2022; Accepted 1 October 2022
Available online 6 October 2022

Scanning Electron Microscopy coupled with Energy Dispersive X-ray spectrometry

methodological approach here presented as an alternative to SABS grown under laboratory conditions. After a proper identification of the biocolonizers in the SAB through taxonomic and morphological observations, the study of the particulate matter accumulated on the SABs of five constructions was conducted under a multi-analytical approach based mainly on elemental imaging studies by micro Energy Dispersive X-ray fluorescence spectrometry (μ-EDXRF) and Scanning Electron Microscopy coupled with Energy Dispersive X-ray spectrometry (SEM-EDS) techniques, trying to reduce the time needed and associated costs. This methodology allowed to discriminate metals that are part of the original structure of the SABs, from those coming from the anthropogenic emissions. The whole methodology applied assisted the identification of the main metallic particles that could be associated with nearby anthropogenic sources of emission such as Zn, Fe, Mn, Ni and Ti by SEM-EDS and by μ-EDXRF Ba, Sb, Sn, Cl and Br apart others; revealing that it could be used as a good alternative for a rapid screening of the atmospheric heavy metals pollution.

1. Introduction

Atmospheric pollutants have been the subject of interest by the scientific community due to their negative impact on human health (Karri et al., 2016), food security (Sun et al., 2017), and terrestrial and aquatic ecosystems (Szynkowska et al., 2018; Tchounwou et al., 2012). The official reports of the World Health Organization indicate that, in different regions of the world, the concentration of particulate matter (PM) harmful to the human health has been increasing in the last years (World Health Organization, 2016). In urban areas, some studies correlate the high amount of PM rich in heavy metals with specific health problems (Combes and Franchineau, 2019; Glencross et al., 2020; Schraufnagel et al., 2019; Sun et al., 2020). Atmospheric particulate matter rich in heavy metals is usually originated from anthropogenic activities (i.e., road traffic, greenhouse effect, industrial activities, thermal power plants, etc.) and natural events (i.e., volcanic eruptions, forest fires, organic matter decomposition, etc.) (Lelieveld et al., 2015; Haikerwal et al., 2015; Zhang and Batterman, 2013; Querol et al., 2007).

Many are the works dealing with the study of atmospheric airborne particulate matter deposition on leaves, trees, lichens, mosses, soils and sediments (Castaneda-Miranda et al., 2020; Roy et al., 2020; Contardo et al., 2020; Boquete et al., 2020; Islam and Saikia, 2020; Chiaia--Hernández et al., 2020), but scarce those which evaluate its impact on building materials (Sesana et al., 2018). Since decades, most of the studies have focused on the evaluation of the influence of acid gases on the state of conservation of construction materials (Grossi and Brimblecombe, 2002; Prieto-Taboada et al., 2013). One of the main pathologies studies since years in historical and contemporary constructions is the formation of black crusts (Di Turo et al., 2016; Morillas et al., 2016; Martínez-Arkarazo et al., 2007; Saiz-Jimenez, 1993). These crusts are usually formed by the sulfation of the calcium carbonate present on the construction material mainly by the action of atmospheric SO_2 (Ruffolo et al., 2015). The final grey/black color of this kind of crusts is associated with the accumulation of airborne particulate matter on its porous structure. All this has motivated some scholars to use this kind of crusts as passive samplers of airborne particulate matter (Morillas et al., 2016) or even as markers of environmental changes (García-Florentino et al., 2020).

Similarly, biofilms show a great affinity to metallic contaminants and other polar or positively charged molecules due to the presence of charged sites in the heteropolymers of the extracellular matrix as a result of the ionization of functional groups, such as carboxyl and amino groups, sulfates, uronic acids, pentoses and deoxysugars (Cheng et al., 2018; Rossi and De Philippis, 2015). In constructions, under adequate environmental conditions of humidity, sunlight, temperature and pH of the substrate, the colonizers frequently form consortia of phototrophic microorganisms (algae and cyanobacteria) and heterotrophs (bacteria, fungi and protozoa) at the solid/air interface that are called subaerial biofilms (SAB) (Gulotta et al., 2018). Phototrophic microorganisms have been considered primary colonizers, conditioning the nature of building material to subsequent grow heterotrophic microorganisms such as fungi (Villa and Cappitelli, 2019; Crispim et al., 2003). Usually, biodeterioration processes involve many groups of microorganisms that co-exist simultaneously in the susbtrate, forming structured, heterogeneous, and genetically diverse communities protected by a 3D exopolysaccharides matrix (Rossi and De Philippis, 2015; Lembre et al., 2012). This last matrix is primarily responsible for the structural and functional integrity of the SAB (Crispim and Gaylarde, 2005) and, at the same time, determines its physicochemical properties. In functional terms, biofilm matrices play an important role in the biosorption of various contaminants, such as heavy metal ions in aquatic and terrestrial environments (Kurniawan and Fukuda, 2022).

SABs can be also formed spontaneously on the surface of constructions and they do not necessarily imply a "biodeteriorative" role as is frequently thought. In this sense, different scholars have reported the neutral or even bioprotective effect of SABs on stones and other constructing materials under certain environmental conditions (Ramírez et al., 2010; Villa et al., 2015, 2016; Zerboni et al., 2022). In these cases, SABs can act as a barrier that blocks the interaction between the construction materials with the atmosphere. This physical barrier prevents the transformation of the original mineralogical composition due to the interaction with other environmental deterioration agents (e.g., acid gases).

Commonly, to evaluate the nature and concentration of the heavy metals in the atmospheric particulate matter, cascade impactors are usually employed (Chang et al., 2000; Botle et al., 2020; Liu et al., 2022; Zhang et al., 2018). This kind of instruments, thanks to the pumping of the air, collect the particles on filters. Some authors have reported the use of lichens and mosses as natural biomonitors or passive samplers of atmospheric heavy metal pollution (Ogunkunle et al., 2016; Salo et al., 2012; Chakrabortty and Paratkar, 2006; Gallego-Cartagena et al., 2021; Lin, 2015; Wannaz et al., 2013). A recent work confirmed the accumulation of heavy metals associated to airborne PM on algae biolfims (García-Florentino et al., 2018a).

Considering these experimental evidences, the use of SABs that grow spontaneously on constructions deserve to be evaluated as a potential cost-effective passive alternative to extract a general and rapid panoramic view of the possible impact of heavy metals-rich airborne PM in urban areas. Appart from the PM sampling procedure, the development of a fast and cost-effective analytical methodology would highly contribute to the whole strategy. This approach could be useful to assist stakeholders in environmental health and urban planning to make quick decisions about the status of air pollution. Moreover, these analytical methodologies could be also useful in the future to assess the ability of green façades including specific biological organisms (e.g., mosses and algae) in the filtering of atmospheric particulate matter (Srbinovska et al., 2021; Paull et al., 2020; Radić et al., 2019).

In this work, to test the ability of SABs retaining atmospheric PM rich in heavy metals, those formed on the façades of constructions from an urban city, such as the one of Barranquilla (Colombia), were considered. To evaluate their role as retainers of atmospheric PM, first, the taxonomic identification of the biocolonizers in the SABs was conducted. Once elementally and mineralogical characterized the plasters/mortars of the façades where the SABs were samples, the airborne PM trapped on them was studied. To this aim, a non-invasive analytical strategy based on elemental imaging analysis, which does not require any sample

preparation has been designed. To evaluate the distribution and abundance of heavy metals present in the particles accumulated in the SABs Scanning Electron Microscopy coupled with Energy Dispersive X-ray spectrometry (SEM-EDS) and micro-Energy Dispersive X-ray Fluorescence spectrometry (μ-EDXRF) was used. The obtained experimental evidences were employed to extract conclusions about the impact of nearby anthropogenic sources contributing to the emission of airborne PM rich in heavy metals.

2. Materials and methods

2.1. Sampling locations, climatic conditions and anthropogenic pollution sources

In order to prevent from possible washing of the PM trapped on the SABs by the action of rain, sampling was carried out during the dry season (December–January) (Zhou et al., 2022; Mariani and de Mello, 2007; Rubio et al., 2001). The samples were collected from the north facing façade, the preferential orientation where the SABs have been formed (Häubner et al., 2006). Concretely, samples from five constructions from the North Historic Center of the Special, Industrial, and Port District of Barranquilla, capital of Atlantic Department (Colombia) were obtained (Fig. 1). In Barranquilla, the tropical savannah climate predominates according to the Köppen-Geiger climate classification with an average annual temperature of 27.1 °C, presenting minimum temperatures of 25.2 °C in February and maximum of 29.4 °C in July. Two moderate wind flows prevail with northeast (42.7%) and north (25%) directions, respectively. Frequencies relative to the East, Southeast and South are also presented, with 5.8%, 6.1% and 6.1% of observations, respectively (IDEAM, 1997). The average annual rainfall is 814 mm, where October reaches the highest rainfall peak with 1396 mm and February the lowest peak with 22 mm. The percentage of annual relative humidity (% RH) is 80%, exhibiting the maximum peak in October with 85.10% and the minimum in February with 78.21%. The mean annual solar luminosity is around 3406.8 h (Agudelo-Castañeda et al., 2020; Ramírez-Cerpa et al., 2017). In addition to the climatic factors of the city described, other environmental factors of an anthropogenic nature coexist that assist the growth of biofilms on the surface of the selected buildings, such as humidity induced by air conditioning devices, irrigation of vertical gardens on terraces and the discharge of water through river gutters (Table S1). The façades of the selected constructions showed signs of aesthetic alterations and deterioration related to biofilms (Fig. S1 until S5).

To select the studied constructions, those areas from the locality with identified sources of anthropic activities that could contribute to the emission of particulate matter rich in heavy metals were considered. Generally speaking, the Historic Center of Barranquilla also suffer the diffuse impact of the recurrent forest fires that usually occur in the Vía Isla de Salamanca Park during the dry season (Nolte, 2016).

The first sampling point (B1) was the building of the *Universidad del Atlántico* headquarters, located in the city's downtown area (Fig. S1). This sampling point is located 50 m from a highway with high road traffic, 100 m from auto shops, and 200 m from fuel (Fig. S1A). The second sampling point (B2) was the *Catedral Metropolitana de*

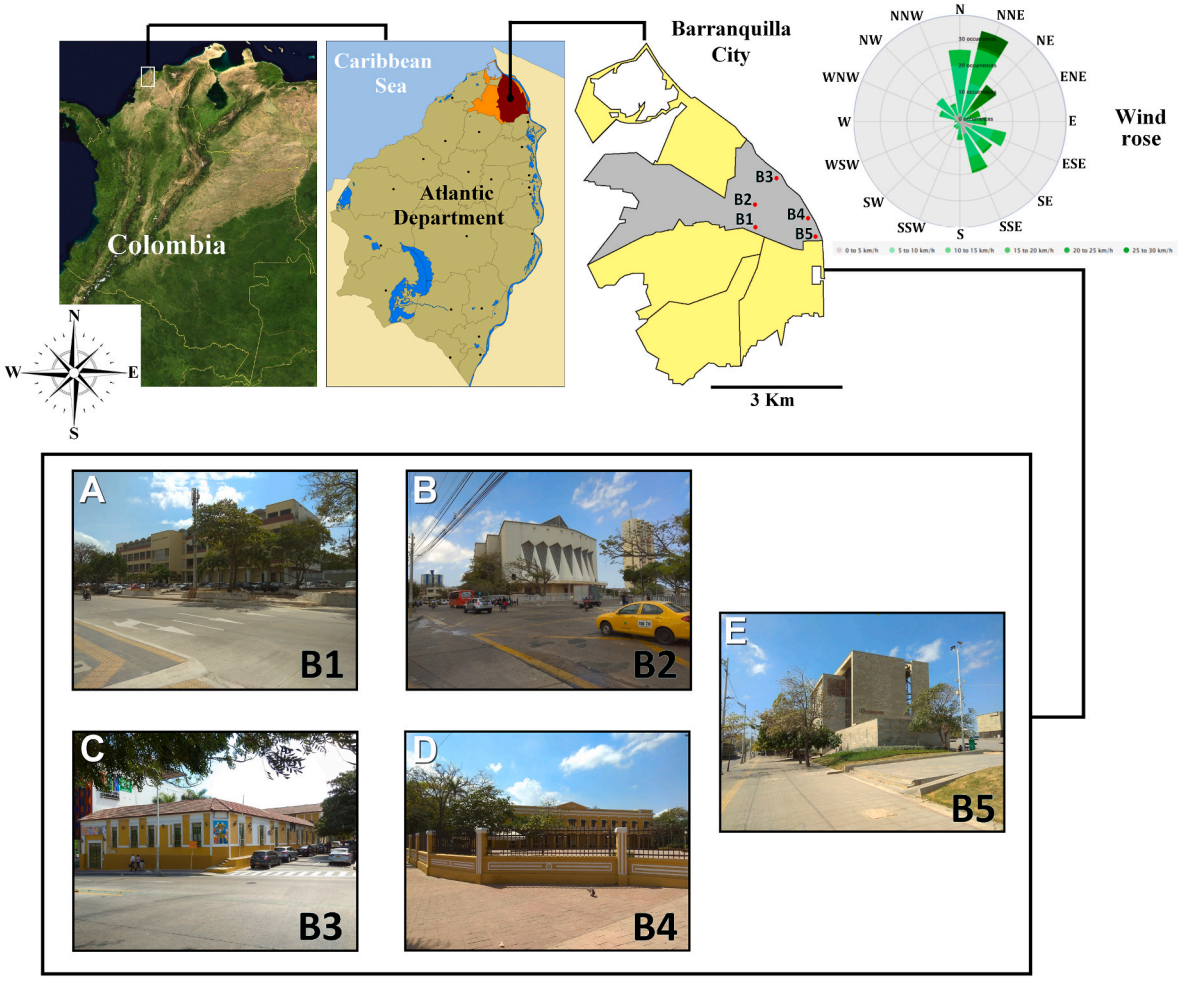

Fig. 1. Location of sampling sites in the Barranquilla city, Colombia. A) Atlantico University headquarters Center (B1); B) María Reina de Barranquilla Metropolitan Cathedral (B2), C) Casa del Carnaval (B3), D) Caribbean Pilot Library (B4) and E) Caribbean Museum (B5).

Barranquilla, located in the city's downtown area (Fig. S2). This sampling point is at a distance of 50 m from an urban road with high traffic, 100 m from an urban bus station and 500 m from the city's industrial complex. The third sampling point (B3) was the historical construction of the *Casa del Carnaval* (Fig. S3). This sampling point is located 300 m from a food and paper processing industry, 50 m from a highway with high vehicular traffic. The fourth sampling point (B4) was the historical construction of the *Biblioteca Piloto del Caribe* (Fig. S4). The building is located 500 m from the city's industrial complex. Among the main sources of contamination are the stock centers for the recycling of metallic materials (100–150 m away) roads with high traffic of medium-load transport vehicles (50 m away) and the presence of a traffic light (70 m away). Finally, the fifth sampling point (B5) was the *Museo del Caribe* building (Fig. S5). This sampling point is located 50 m from an urban bus station and a road with high vehicular traffic, 100 m from shopping centers with high pedestrian traffic, and 200 m from a recycling stock center for metallic materials.

2.2. SABs sampling and description

Considering the historic value of the constructions and in order to minimize the damage during samplings, three small fragments of 4–9 x 4–9 mm^2 from the areas colonized by the SABs from each construction respectively were taken. The samples were randomly extracted from the first 2 m heigh of the façade considering the floor as zero. To characterize the elemental and mineralogical composition of the mortars/substrates where SABs have been formed, also three mortar fragment of less than 10 × 10 mm^2, from each construction respectively, were randomly taken from areas not affected by the SABs but close to them. For the sampling of the areas colonized (SABs) sterile scalpel blades were used, cleaning from one to each sampling. For the mortar fragments extraction, a hammer and a chisel were used. The samples of construction material colonized with biofilms were stored in plastic microtubes. The samples of construction material without colonization were stored in Ziploc bags and preserved in Petri dishes.

For the growth and subsequent taxonomic characterization of eukaryotic and prokaryotic algae, biofilm scrapings were conducted on the SABs and the scrapped material was introduced into Eppendorf vials enriched with Guillard's medium f/2 and BG-11. Such vials were placed in a culture chamber for 12 day at a temperature of 28 °C ± 2 °C, pH 7.5 ± 1.2 and a photoperiod of 8 h of light and 16 h of darkness, respectively. After this time, samples of algae and cyanobacteria developed with a Pasteur micropipette were taken from the culture vials and placed on slides for observations under an optical microscope, and taxonomic identification was carried out through morphological descriptions and implementation of taxonomic keys suggested by different scholars (Anagnostidis and Komárek, 1988; Anagnostidis, 1986; López-Bautista et al., 2007; Prescott, 1964).

In the case of SAB samples intended for the identification of heterotrophic microorganisms (fungi), biofilm scraping samples were inoculated in triplicate in Petri dishes enriched with Sabouraud Agar Glucose and Chloramphenicol Glucose Agar culture media (Merck, Germany). The inocula were incubated in a model E23 oven (BINDER, Germany) at 30 °C for 5 days. After this time, each sample was subjected to the Ridell technique to facilitate the selection and handling of the developed colonies (Weber and Pitt, 2000). The microscopic fungal samples were separated from the colonies with clamps and placed on a slide with a drop of lactophenol or tween 20. For morphological descriptions, microscopic observations the structures (for example, type of mycelia, presence of septa, etc) with 10X and 40X objectives were made. In the case of observing spore ornamentation and color, a 100X immersion objective was used. The interpretation and analysis of the morphological characteristics and taxonomic identification were carried out according to the studies presented elsewhere (Bartnicki-Garcia, 1968; Kidd et al., 2016).

2.3. Instrumentation

The mineralogical characterization of the mortars by means of X-ray diffraction (XRD) previously required the pulverizing of the samples by manual grinding in an agate mortar. For the XRD analyses, 0.5–1.0 g were used per sample. One sample was generated from each of the three mortar samples obtained from each building. The samples were idependently analyzed showing the representative results obtained from the three of them. The analyses were conducted using a powder diffractometer PANalytical Xpert PRO instrument equipped with a copper tube ($\lambda_{CuK\alpha media}$ = 1.5418 Å, $\lambda_{CuK\alpha1}$ = 1.54060 Å, $\lambda_{CuK\alpha2}$ = 1.54439 Å), a vertical goniometer (Bragg-Brentano geometry), a programmable divergence aperture, an automatic interchange of samples, a secondary monochromator of graphite and a PixCel detector. The measurement conditions were 40 kV and 40 mA, with an angular range (2θ) scanned between 5 and 70°. Moreover, X'pert HighScore (PANalytical) software combined with the specific powder diffraction file database (International Centre for Diffraction Data-ICDD, Pennsylvania, USA) was used for the data treatment of the diffractograms and the identification of the present mineral phases.

The elemental analysis of the SABs and their corresponding mortar was conducted using the EDXRF spectrometer M4 TORNADO (Bruker Nano GmbH, Berlin, Germany). With this instrument, multi-point and imaging analyses were conducted. For the quantitative elemental analysis of the mortars, one pressed pellet was prepared from each of the three samples. A multi-point measurement strategy was used. Fifty points randomly distributed were programmed in each pellet at a lateral resolution of 1 mm. Measurements were acquired during 300 s using an Rh tube operating at 50 kV and 700 μA. The quantitative elemental information was obtained using previously optimized empirical calibrations described elsewhere (García-Florentino et al., 2018b). For certain elements (Co, V, Cr, Ni, Cu, Br, As and Ba) semi-quantitative information was only possible to obtain. Results were calculated as the average of the results obtained from the three analyzed pellets from each sampling location.

To study the SABs, multi point and imaging analyses were conducted. For the imaging study, a microfocus side window Rh tube powered by a low-power H.V. generator and cooled by air was used. Thanks to the implemented poly-capillary lens, measurements were acquired at down to 25 μm of lateral resolution. The spot size varies as a function of the energy, 17 μm at 2.3 keV and 32 μm at 18.3 keV. For spectral acquisition, the X-ray tube was programmed at its maximum voltage and current of 50 kV and 600 μA, respectively. The detection of the fluorescence radiation was performed by an XFlash silicon drift detector with 30 mm^2 sensitive areas and an energy resolution of 145 eV for Mn-Kα. To improve the detection of the lightest elements (Z < 11), filters were not used, and measurements were acquired under vacuum (20 mba) using the diaphragm pump MV 10 N VARIO-B. For the focus of the area under study, two video microscopes were used to explore the sample under low magnification (1 cm^2 area), and the other one to perform the final focusing (1 mm^2 area). The elemental distribution maps were obtained after the deconvolution of the sum spectrum of the whole mapped area, and they were shown according to the K_α line of each element except for Pb, for which the L_α line was used. The acquisition and processing of the individual spectra and mappings were conducted using the ESPRIT family software (Bruker Nano GmbH, Berlin, Germany). In this work, the most representative distribution maps are shown. Selected samples of SABs were scrapped from the mortar acting as substrate, and they were analyzed following the multipoint strategy previously described for the mortar samples. In this case, only semi-quantitative results were obtained.

Elemental distribution maps obtained through μ-EDXRF were also used to compare, which are the heavy metals present at higher concentrations in each SAB obtained from each construction. For that, the concentration (semi-quantitative values) of each heavy metal detected was divided by the area of studied SAB sample. As three samples were

maped from each constructions, the results were offered in μg/g/mm^2 together with the standard deviation. For the comparative study, as the constructions from which the samples B1, B2 and B3 are coetaneous, we assume that SABs would have formed in a similar period of time. In contrast, the construction from which B5 samples were taken, was recently erected. This last has been taken into account in the comparison of the numerical values obtained.

To determine the composition of the individual particles and aggregates accumulated in the SABs, SEM-EDS analyses were also conducted. The selected samples were mounted on an aluminum pin stub fixed to a carbon tape. The three SAB samples from each location were visualized under the SEM in order to select the one with a higher number of particles deposited as the representative and considered one for the analyses. For the image acquisition, the surfaces of SABs were coated with gold to ensure their conductivity and, therefore, to obtain microscopic images of good quality. For the SEM-EDS analyses, an EVO®40 Scanning Electron Microscope (Carl Zeiss NTS GmbH, Germany) coupled to an XMax Energy-Dispersive X-ray spectrometer (Oxford Instruments, Abingdon, Oxfordshire, United Kingdom) was used. SEM images were obtained at a low vacuum employing an acceleration voltage of 30 kV and a 10–400 μm working distance for the image acquisitions and elemental analysis (single point and imaging). Different magnifications (reaching up to 6800X) were used for secondary electron images, and an integration time of 50 s was employed to improve the signal-to-noise ratio. The EDS spectra were acquired and treated using the INCA suite software (version 4.13) (Oxford Instruments, Abingdon, Oxfordshire, United Kingdom).

3. Results and discussion

3.1. Identification of the microorganisms present in the SABs

Phototrophic microorganisms at sampled locations showed a light green to dark green or grayish patchy distribution on the building surface. These surfaces were often affected by humidity due to water retained within the substrates, splashing of water by rain gutters, or garden irrigation activities (Table S1 and Fig. S1 until Fig. S5).

The SAB samples analyzed in this study are compact filamentous matrix, with a regular shape totally distributed on the surface of the mortars (Fig. 2a). Exceptions are the samples B4 (Fig. 2c) and B5 (Fig. 2b). The first one represents a black non-filamentous compact matrix and the second one shows a non-compact and diffuse structure.

Microscopic, morphological, and taxonomic analysis of the microorganisms isolated from the SABs indicated the presence of ten phototrophic microorganisms and four type of fungi (Table 1). In this study, it was possible to identify eight bacteria from Phylum Cyanobacteria in each analyzed SAB sample. The identified cyanobacteria genus were *Phormidium* sp., *Oscillatoria* sp., *Chroococcus* sp., *Gloeocapsa* sp., *Cyanosarcina* sp., *Leptolyngbya* sp., *Lyngbya* sp. and *Asterocapsa* sp. Additionally, in the B5 sample, *Chlorella* sp. and *Trentepohlia* sp. from Phylum Chlorophyta were also identified. In the majority of the SAB samples, fungal species such as *Aspergillus niger*, *Aspergillus fumigatus*, *Penicillium* sp., and *Fusarium* sp. from Phylum Ascomycota were identified.

Observations of the phototrophic microorganisms collected from the biofilms under the light microscope revealed the presence of filamentous forms of *Phormidium* sp., *Oscillatoria* sp., *Leptolyngbya* sp. and *Lyngbya* sp. (Fig. S6) while under canopy the coccoid cyanobacteria *Chroococcus* sp., *Cyanosarcina* sp., *Asterocapsa* sp. and *Gloeocapsa* sp. were observed in most of the samples (Fig. S7).

Fungal activity is significantly higher in tropical climates (high temperatures and humidity), such as the one of Barranquilla (Pinto et al., 2019). Concretely, in the SABs under study an extended presence of fungi from Phylum Ascomycota with a higher-prevalence of the species *A. niger*, *A. fumigatus,* and the genera *Penicillium* sp. and *Fusarium* sp was observed. In the SABs, (Fig. S8), these microorganisms successfully growth due to their synergistic interaction with cyanobacteria (Gaylarde, 2020; Scheerer et al., 2009; Cutler and Viles, 2010).

Sample B5 can be considered a specific case in which *Chlorella* sp. and *Trentepohlia* sp. algae were identified as accessory species among the abundant composition in the SAB of filamentous (*Phormidium* sp., *Oscillatoria* sp. and *Lyngbya* sp.) and coccoid cyanobacteria *Gloeocapsa* sp. The presence of cyanobacteria with hyaline or gelatinous envelopes likely favors the fixation to the substrate of the identified fungal and phototrophic microorganisms. Experimental studies indicate that *Chroococcus* sp. has a reasonably thick mucus layer that promotes the maintenance of Chlorophyta agglomerations such as *Chlorella* sp. and

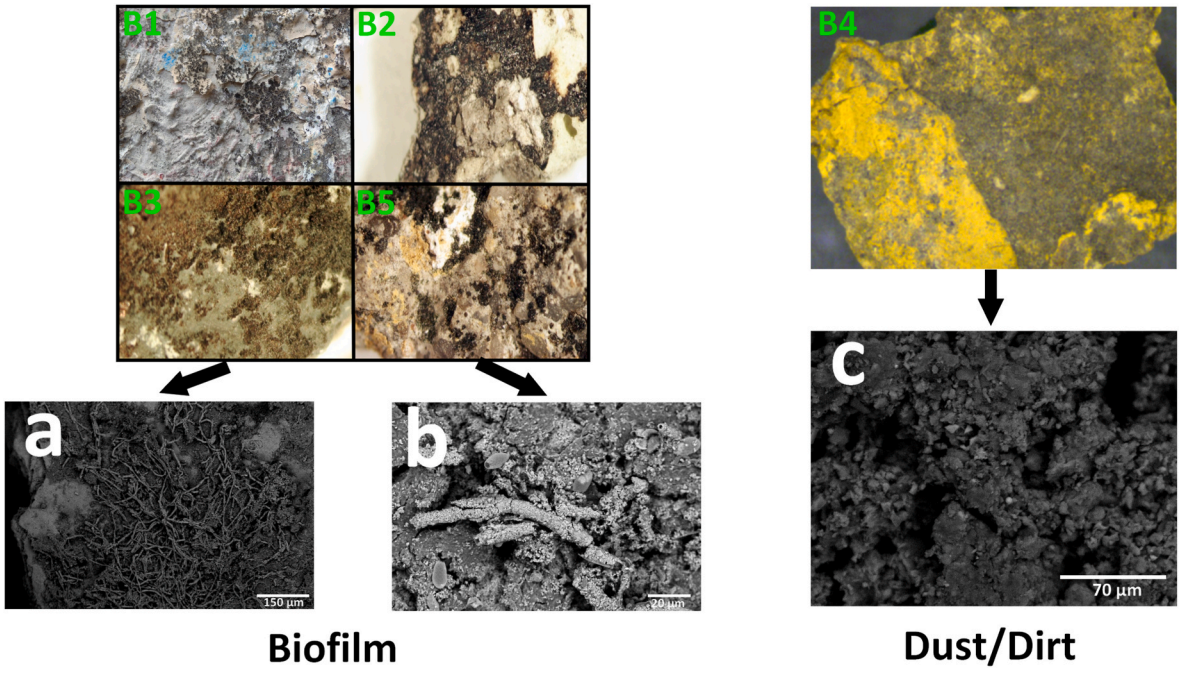

Fig. 2. Distribution and structure of biofilms. A) Structure of the filamentous biofilm (B3) distributed on the surface of the mortars. B) Structure of the filamentous biofilm (B5) with diffuse distribution and not very compact. C) Non-filamentous compact matrix with regular distribution on the surface of the substrate (B4).

Table 1
Phototrophic microorganisms and fungi associated with biodeterioration in historical buildings from Barranquilla.

Samples	Phototrophic microorganisms		Fungi Division Ascomycota	Aesthetic alteration and biodeterioration
	Phylum Cyanophyta	Phylum Chlorophyta		
B1	*Phormidium* sp., *Oscillatoria* sp., *Chroococcus* sp., *Cyanosarcina* sp.,	-	*Aspergillus niger*, *Aspergillus fumigatus*, *Penicillium* sp., *Fusarium* sp.	Green, brown to black patinas and heavy discoloration, cracks, flakes off and swelling of walls. Black patinas, heavy discoloration and cracks on walls and balcony.
B2	*Asterocapsa* sp., *Phormidium* sp., *Oscillatoria* sp.	-	*Aspergillus niger*, *Aspergillius fumigatus*, *Penicillium* sp., *Fusarium* sp.	Black patinas and heavy discoloration on walls
B3	*Chroococcus* sp., *Phormidium* sp., *Oscillatoria* sp., *Cyanosarcina* sp., *Gloeocapsa* sp.	-	*Aspergillus niger*, *Aspergillius fumigatus*, *Penicillium* sp., *Fusarium* sp.	Black patinas, heavy discoloration and light flake off on walls.
B4	*Chroococcus* sp. *Phormidium* sp., *Leptolyngbya* sp., *Lyngbya* sp.	-	*Aspergillus niger*, *Aspergillus fumigatus*, *Penicillium* sp.	Green, brown to black patinas and heavy discoloration, cracks, flakes off and swelling of walls.
B5	*Phormidium* sp., *Oscillatoria* sp., *Gloeocapsa* sp., *Lyngbya* sp.	*Chlorella* sp., *Trentepohlia* sp.	*Aspergillus niger*, *Aspergillus fumigatus*, *Penicillium* sp., *Fusarium* sp.	Black patinas and heavy discoloration on walls

Stichococcus bacillaris in substrates of urban buildings and monuments (Gallego-Cartagena et al., 2020; Vojtková, 2017; Crispim et al., 2003; Gaylarde and Gaylarde, 2002).

3.2. Mineralogical characterization of the constructions materials

In the mortars analyzed by XRD, the major crystalline phases identified were quartz (α-SiO_2) and calcite ($CaCO_3$), although, in samples B1, B3, and B5, plagioclases ($NaAlSi_3O_8$–$CaAl_2Si_2O_8$) and potassium feldspars ($KAlSi_3O_8$) were also identified (Table S2). According to the XRD results, these materials can be related to calcareous mortars. Tremolite ($Ca_2Mg_5Si_8O_{22}(OH)_2$), dolomite ($CaMg(CO_3)_2$), and rutile (α-TiO_2) were also detected in sample B2, while gypsum ($CaSO_4{\cdot}2H_2O$) in sample B4. The presence of tremolite ($Ca_2Mg_5Si_8O_{22}(OH)_2$) in building materials is associated with fibrous materials related to asbestos (for example, stucco with asbestos), still used as feedstock in the preparation of filler for decorative coating, protection, and sound-isolating on the façades of buildings in some countries (Paglietti et al., 2016; Bloise et al., 2008). It should be highlighted that during the sample preparation, when grinding B2 sample before XRD analysis, a mechanical behavior of plastic/ductile nature was observed in the sample. The presence of rutile (α-TiO_2) in B2 sample could be related to the paint layer applied on the surface of the facade. The identification of gypsum in sample B4 could also be related with its intentional addition in the mortar or due to a sulfation process of the calcium carbonate of the mortar.

3.3. Elemental composition of the construction materials

EDXRF analysis of the internal part (not exposed to the atmosphere) and the external part (exposed to the atmosphere) of the mortars allowed to detect major elements such as Mg, Al, Si, P, S, Cl, K, Ca and Fe and minor elements such as Ti, Mn, Zn, Rb, Sr, Pb (Table 2).

The high concentrations of Ca and Si in the samples are related to calcite and quartz presence resulting from the fine aggregate of the mortar. The highest concentrations of Al, Si, and K are related to the aggregates of mortars rich in aluminosilicates (plagioclase and feldspars).

Significant differences in the concentration of some major elements were observed comparing the external and internal parts (Tables 2 and 3). Remarkable is the higher concentration of Fe (24.0 ± 3.0%) in the external part of the mortar of B5 sample, which shows an increase of concentration up to 72%. In this sample, a blackish dust was observable on the external part of the mortar, which could be associated to depositions of airborne particulate matter rich in Fe. In general terms, the increase of Fe comparing the external and internal parts of the mortars from all the samples represents a 62 ± 7% as an average value. Moreover, external parts of the mortar in sample B2 and B4 are especially rich in Ti (concentrations of 24.6 ± 3.1 and 32.7 ± 4.1 % respectively) due to the use of TiO_2 as coating in these external mortars/plasters.

Zn was under the Limit of Quantification in the internal part of all the mortar samples. However, in the external parts, its concentration range from 0.1 to 0.01% depending on the sample (Tables 2 and 3).

Pb was not detected or it is set below the Limit of Quantification in the internal parts of all the samples. On the contrary, in the external parts of samples B1 and B2, this heavy metal was detected at concentrations higher than 0.01%. The same trend was observable for Mn in the external parts of mortar samples B1 and B5 with increments of 76 and 100% respectively. The increase of chlorine in the external parts of samples B2 and B5 could be related to the diffuse influence of the marine aerosol or to an irregular distribution of Cl in the mortar due to capillary rise of water rich in chlorides (Table 2).

3.4. Study of the nature and distribution of the airborne particulate matter rich in metals in the SABs through elemental imaging

The elemental imaging study by μ-EDXRF allowed to determine the distribution of metals accumulated on the SAB. To start, direct imaging analyses were conducted, being able to detect the following elements in all the SABs: Mg, Al, Si, P, S, K, Ca and Fe as major elements; and Ti, Mn, Zn, Rb, Sr, Pb, Cu, V, Cr and Ni, as minor/trace elements up to some μg/g (Figs. 3 and 4; Table 4). As a SAB can be considered a light material, due to the penetration ability of the X-Rays, to ensure that the mortar below the SAB do not contribute to the final result, SAB samples B1 and B4 (considering the three samples extracted from each location) were selected for an additional test. In these samples, the SABs were separated from the mortar scraping and separating their mass. The isolated mass of the SAB samples was independently analyzed through a multi-point strategy being possible to detect the same elements identified through the direct measurements of the SABs on the mortars (Table S3 and Fig. 4).

The semiquantitative results obtained in the scraped SABs indicate that P and S concentrations were lower in sample B4 (0.82 ± 0.15%) compared with the sample B1 (8.54 ± 3.21%) (Table S3). The same was observed for S (0.88 ± 0.29% in B4 vs. 8.00 ± 1.83% in B1) (Table S3). As P and S are representative elements of the constitution of biological matrices, the low concentration of these elements in B4 suggests that it cannot be considered a structurally constituted SAB although biocolonizers were identified on it. Indeed, at the naked eye, the crust does not show a filamentous structure (Fig. 2c). The especially high concentration of specific heavy metals (Ti, Cr, Fe, Ni, Zn, Pb) (Table S3) in B4 suggests that this crust has been formed due to the deposition of atmospheric airborn particulate matter (particles coming from soiling

Table 2
Concentration of major elements (norm. wt.%) in the external or exposed parts (EP) and internal or non-exposed parts (IP) of the mortar samples without the influence of the SABs.

Samples	Mg		Al		Si		P		S		Cl		K		Ca		Fe	
	EP	IP	EP	IP	EP	IP	EP	IP	EP	IP	EP	IP	EP	IP	EP	IP	EP	IP
B1	<LOQ	<LOQ	9.7 ± 2.0	2.5 ± 0.5	40.7 ± 5.1	10.5 ± 1.9	<LOQ	<LOQ	1.3 ± 0.3	0.3 ± 0.2	<LOQ	N.D	2.3 ± 0.5	0.7 ± 0.3	40.7 ± 4.9	85.2 ± 10.0	4.6 ± 0.8	0.7 ± 0.2
B2	5.2 ± 0.9	7.0 ± 1.6	5.7 ± 0.9	1.2 ± 0.8	18.5 ± 1.9	4.8 ± 0.8	0.9 ± 0.4	<LOQ	1.4 ± 0.3	0.7 ± 0.2	2.4 ± 0.2	<LOQ	0.9 ± 0.1	0.1 ± 0.0	37.9 ± 1.8	86.2 ± 10.0	2.4 ± 0.2	<LOQ
B3	<LOQ	<LOQ	10.6 ± 3.0	9.7 ± 1.9	34.1 ± 8.0	36.9 ± 5.8	<LOQ	<LOQ	1.1 ± 0.1	0.7 ± 0.1	<LOQ	<LOQ	3.0 ± 0.6	2.3 ± 0.6	45.4 ± 1.7	47.0 ± 4.0	4.5 ± 0.2	2.7 ± 0.7
B4	2.5 ± 0.8	3.5 ± 1.5	18.7 ± 3.5	5.0 ± 1.4	18.2 ± 1.6	15.3 ± 4.9	<LOQ	0.4 ± 0.2	0.7 ± 0.1	2.1 ± 0.9	0.5 ± 0.1	1.0 ± 0.4	0.5 ± 0.1	0.6 ± 0.1	24.8 ± 3.1	67.6 ± 9.0	1.2 ± 0.2	3.7 ± 0.8
B5	5.2 ± 1.3	<LOQ	8.7 ± 1.3	3.9 ± 0.4	16.3 ± 1.5	5.8 ± 0.4	0.3 ± 0.1	<LOQ	0.3 ± 0.1	0.5 ± 0.0	0.5 ± 0.1	N.D	1.2 ± 0.4	0.3 ± 0.1	42.9 ± 5.2	82.4 ± 10.0	24.0 ± 3.0	6.8 ± 1.4

<LOQ: Under the Limit of Quantification **N.D:** Non-detected.
Errors are expressed as one time the standard deviation of the mean concentration calculated from the values obtained from the three individual samples from each sampling location.

Table 3
Concentration of minor/trace elements (norm. wt.%) in the external or exposed parts (EP) and internal or non-exposed parts (IP) of the mortars samples without the influence of the SABs.

Samples	Ti		Mn		Zn		Rb		Sr		Pb	
	EP	IP	EP	IP	EP	IP	EP	IP	EP	IP	EP	IP
B1	0.6 ± 0.2	0.06 ± 0.02	0.14 ± 0.11	0.03 ± 0.01	0.01 ± 0.01	<LOQ	0.006 ± 0.002	N.D	0.12 ± 0.08	0.02 ± 0.01	0.02 ± 0.01	N.D
B2	24.6 ± 3.1	0.04 ± 0.01	0.04 ± 0.01	0.06 ± 0.02	0.08 ± 0.03	<LOQ	<LOQ	N.D	0.02 ± 0.01	0.03 ± 0.01	0.04 ± 0.01	N.D
B3	1.0 ± 0.2	0.4 ± 0.1	0.13 ± 0.07	0.09 ± 0.03	0.02 ± 0.01	<LOQ	<LOQ	<LOQ	0.11 ± 0.05	0.01 ± 0.01	<LOQ	<LOQ
B4	32.7 ± 4.1	0.6 ± 0.1	<LOQ	0.10 ± 0.02	0.015 ± 0.007	<LOQ	<LOQ	N.D	0.30 ± 0.15	0.15 ± 0.02	<LOQ	N.D
B5	0.9 ± 0.3	0.27 ± 0.03	0.03 ± 0.02	<LOQ	0.03 ± 0.01	<LOQ	<LOQ	N.D	0.06 ± 0.03	0.07 ± 0.01	<LOQ	<LOQ

<LOQ: Under the Limit of Quantification N.D: Non-detected.
Errors are expressed as one time the standard deviation of the mean concentration calculated from the values obtained from the three individual samples from each sampling location.

and anthropogenic activities). Among all the samples, only in B4 lead was detected as part of the deposited crust.

In general, SAB samples showed the presence of heavy metals such as Cu, V, Cr, and Ni, not detected in the mortar itself (Tables 2–3). μ-EDXRF imaging revealed that S is homogeneously distributed (Fig. 3) in the SABs, confirming its relation with the structure of the biocolonizers. In contrast, Fe and Ti (specially in samples B2 and B5), Mn (in B1, B3 and B4), Cr (in B2 and B4), Zr (in B1 and B5) are heterogeneously distributed as hot spots on the mentioned SABs. Furthermore, a similar distribution was detected for elements such as Ni, in B4 and Zn in B2, B3 and B5 (Fig. 3). Moreover, B4 sample was the only one in which Pb was detected (Table S3 and Fig. 3) in very punctual areas, confirming that this heavy metal is part of the PM that forms the previously mentioned crust.

3.5. SEM-EDS study of single particles and clusters accumulated in the SABs

In order to examine the elemental composition of single-particles and clusters (aggregated particles) at a lower lateral resolution, single point and imaging SEM-EDS studies were also conducted. 128 particles in total were studied on the SABs from all construction (Table 5, Table S4, Figs. 5–7 and Fig. S9).

71% of the total particles analyzed belong to individual ones with diameters ranging from 2 to 40 μm, while the particles that form clusters correspond to 29% with diameters from 20 to 80 μm (Table 5 and Table S4). 56% of the particles are in the range of PM_{10} and 21% are close to $PM_{2.5}$ size, a high percentage considering that the lower size particles are the ones that could generate adverse effects for human health.

The highest number of individual particles were identified in SABs B1 and B2. A higher percentage of clusters were detected in B1, B2 and B3. Heavy metals such as Fe, Mn, Ni, Cr and Ti were identified on individual particles, with sizes ranging from 5 to 40 μm (Table 5, Figs. 5–7 and Fig. S9d). This result agrees with the identification of hot spots of these metals by μ-EDXRF (Fig. 3). Specifically, Fe, Ti and Ni were detected in a higher proportion in B1 and B2 samples (Table 3). Ti-rich particles detected by SEM-EDS on the SABs could be related to the TiO_2 coating paint that has flaked off the building material or to activities related to iron welding and auto mechanic workshops that take place near the constructions where the SABs were extracted (Andrade-Guel et al., 2022). In addition, Fe–Ti–Mn-rich spherical particles were occasionally observed in the SAB filaments (Fig. 5b–d and Fig. S9). These particles are possibly emitted by the metallurgical industries and the combustion of petrochemical products derived from vehicular traffic (fuel oil, automobile oil) (Wang et al., 2021; Mitsos et al., 2022).

In the cluster particles, elements such as Al, Si, Ca, Mg, Na, Cl, Fe, K, Ti, Cu, Zn, Ba, Pb, Cr, Mn, Br, Ni, Sn, Sb and V were detected (Table 5). As bromine was not observable by μ-EDXRF, its presence can be

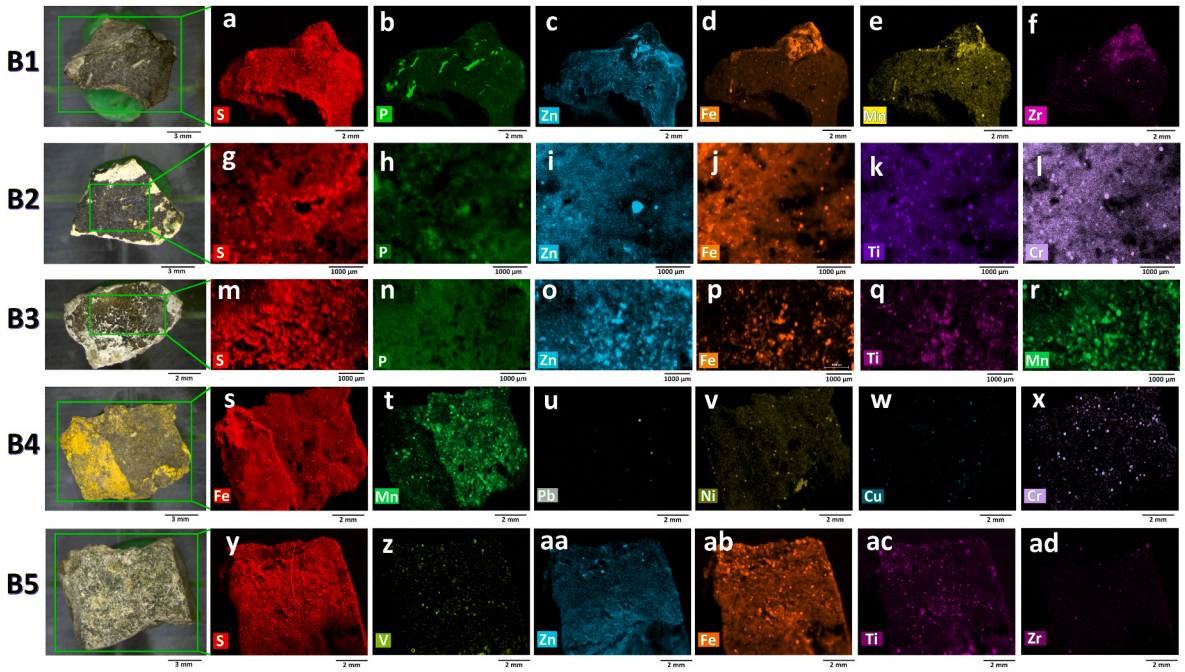

Fig. 3. μ-EDXRF imaging of SAB samples. Elemental distribution maps of sample B1: a) S b) P c) Zn d) Fe e) Mn f) Zr Elemental distribution maps of sample B2: g) S h) P i) Zn j) Fe k) Ti l) Cr. Elemental distribution maps of sample B3: m) S n) P o) Zn p) Fe q) Ti r) Mn. Elemental distribution maps of sample B4: s) Fe t) Mn u) Pb v) Ni w) Cu x) Cr. Elemental distribution maps of sample B5: y) S z) V aa) Zn ab) Fe ac) Ti ad) Zr.

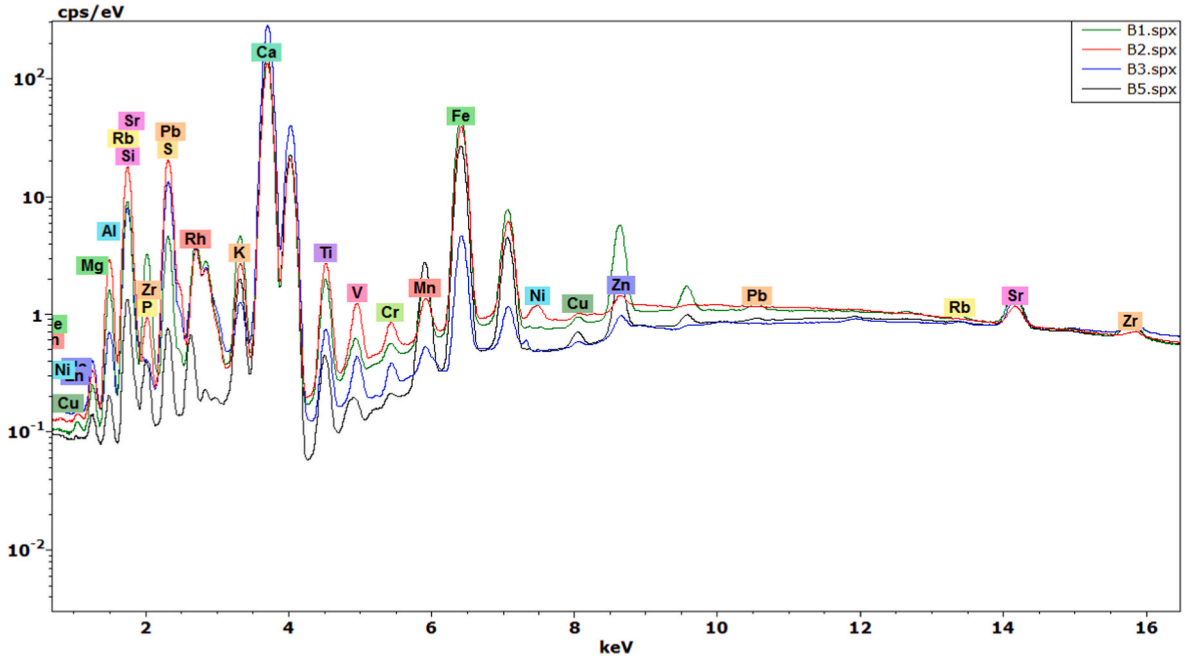

Fig. 4. Representative XRF spectra obtained from SAB samples.

considered punctual. In Figs. 5b, 6 and 7b, 7d and S9b examples of possible clustering of particles coming from geogenic or soiling of minerals/stones (Ca, Al and SO) and those emitted in anthropogenic activities (metallic particles rich in Ti, V, Cr, Ba, Fe and Ni) are observable. The diffuse influence of the marine aerosol was also confirmed by the identification of NaCl particles (see as an example in Fig. 5a, the particle deposited 8–10 μm diameter in the filamentous structure of the SAB of sample B1). The punctual presence of this kind of particles and their size, which is set under the lateral resolution of the μ-EDXRF spectrometer explains the non-detection of chlorine in B1 by this last mentioned technique.

In Fig. 6, an additional example of a cluster detected in the SAB of sample B2 is presented. Elements associated to crustal particulate matter (Al, Si, K and Ca mainly) and smaller metallic particles (even with sizes < than 10 μm) of Fe and Ni were detected. These two metals were also identified as hot spots in the same sample by μ-EDXRF. Regarding Ni, this last has also been identified in clusters together with Al, Ca, Si, Ti, Fe, Mn, Mg and Cr in samples B3 and B5 (Figs. 6 and 7a-b; Figs. S9b and S9e and Table 5).

The identification of clusters including Na–Cl (Fig. 5a), elements

Table 4
Heavy metals concentrations as a function of the area mapped in each SAB by μ-EDXRF (μg/g/mm^2 units).

SAB sample	Fe	Ti	Mn	Zn	Rb	Sr	Pb	Cu	V	Cr	Ni
B1	0.3010 ± 0.0053	0.0280 ± 0.0010	0.0104 ± 0.0009	0.0271 ± 0.0012	0.0003 ± 0.0001	0.0059 ± 0.0018	0.0023 ± 0.0005	0.0008 ± 0.0002	0.0008 ± 0.0001	0.0012 ± 0.0003	ND
B2	0.4071 ± 0.0105	0.0662 ± 0.0027	0.0111 ± 0.0008	0.0037 ± 0.0014	[a]	0.0046 ± 0.0017	0.0005 ± 0.0001	0.0009 ± 0.0001	0.0120 ± 0.0012	0.0040 ± 0.0012	0.0029 ± 0.0004
B3	0.0406 ± 0.0035	0.0151 ± 0.0004	0.0029 ± 0.0010	0.0024 ± 0.0009	0.0004 ± 0.0001	0.0140 ± 0.0020	0.0002 ± 0.0001	0.0005 ± 0.0001	0.0034 ± 0.0006	0.0015 ± 0.0004	ND
B5	0.1801 ± 0.0023	0.0073 ± 0.0005	0.0207 ± 0.0021	0.0066 ± 0.0018	0.0002 ± 0.0001	0.0055 ± 0.0018	0.0006 ± 0.0001	0.0009 ± 0.0001	0.0004 ± 0.0001	0.0003 ± 0.0001	ND

Average mapped areas calculated from the three samples extracted from each sampling location (**B1:** 38.0 ± 1.1 mm^2, **B2:** 17.8 ± 0.8 mm^2, **B3:** 21.9 ± 1.9 mm^2 and **B5:** 45.5 ± 2.1 mm^2).
[a] Lower than 0.0001.

coming from crustal particles (Si, Ca, etc.) and other metals is a clear example of the combine diffuse influence of marine aeorosol, geological influence and anthropogenic activity (see cluster particles of Ti–Fe–Cr and Si–Fe–Cu in sample B1, Fig. 5b and Fig. S10a). Moreover, a combined influence of crustal particles and those emited from anthropogenic sources is clearly visible, as an example mention the detection of Ca–Ni in samples B2 and B3 (Fig. 7a and Fig. S9b), Si–Ca–Ti–Fe in sample B5 (Fig. 7e), Ca–Al–Si–K –Ni–Fe in sample B2 (Fig. 6), Fe–Mn–Cr in sample B4 (Fig. 7b), Si–Ca–Ni–Fe in sample B5 (Fig. S9e), S–Ba–Ca in sample B5 (Fig. 7d), and spherical particles of Fe with Ca contribution in sample B3 (Fig. 5d). All the metals detected corresponde to the ones identified by imaging EDXRF.

It is also remarkable that S and Ba were detected in all samples, although with a higher order of magnitude (<1%) in sample B2, B3 and B5 (Table 5). Particles rich in S–Ba could be related to barium sulfate, which is produced by the wear of automobile brakes, including the abrasion of the material of the brake pads and brake discs, caused by the grinding of the components of the brakes pads or the volatilization and condensation of the brake pad material (Carrero et al., 2013, 2014; Zafra et al., 2016; Pant and Harrison, 2013).

3.6. Correlation of the main anthropogenic emission sources according to the main metals accumulated in the SABs extracted from each construction

To extract additional information about the main metals accumulated on the SABs, and the possible emission sources, as a function of the location of the construction in the city of Barranquilla, the concentration of metals as a function of the mapped area of the SAB by μ–EDXRF was calculated (Table 4). As sample B4 was not defined as a SAB, it was not considered in this case. Moreover, results associated to heavy metals detected are only presented, the values associated to lighter elements have been removed from Table 4 for a better comprehension.

In this sense, the SAB B1 shows the highest concentration of Pb (0.0023 ± 0.0005 μg/g/mm^2) and high concentration of Fe (0.3011 ± 0.0053 μg/g/mm^2) and Cr (0.0012 ± 0.0003 μg/g/mm^2). The first two heavy metals can be associated to the emissions coming from road traffic. Some researches indicate that fine inhalable particles with diameters lower than 1 μm, rich in Fe and Pb, are generated in high temperatures processes derived from vehicular transport; among these, the burning of fossil fuels, tire and engine wear (Machado et al., 2008; Liu et al., 2014). The construction from which B1 sample was obtained is located in a locality of the metropolitan area highly influenced by a continuous traffic, specially coming from public transport. Moreover, this construction presents a poor conservation state due to lack of maintenance and restoration actions.

The SAB B2 corresponds to a construction that presents a relatively better state of conservation. In this case, the highest concentration of Fe (0.4071 ± 0.0105 μg/g/mm^2) and Ti (0.0662 ± 0.0027 μg/g/mm^2) were registered. Moreover, this was the only SAB that showed the presence of Ni (0.0029 ± 0.0004 μg/g/mm^2) (Table 4). The high concentrations of such metals determined by μ-EDXRF in this sample agree with the elemental composition of the single particles (2–12 μm) and cluster (7–80 μm) studied by SEM-EDS in this sample. Additionally, apart from Fe, Zn is also widely present in this sample. These last elements, together with Ni can be associated with fine particle emissions from continuous traffic generated by public transport (Fig. 3, Tables 4 and 5). Additional authors (Osorio-Martinez et al., 2021; Vianna et al., 2011; Poulakis et al., 2015) have proposed that the fine and coarse fractions of PM rich in metals such as Ti, Mn, Cu, V and Ni come from emissions from mixed anthropogenic activities (industry and transport) or geogenic (soil and urban dust) on tropical citys. All this elements are present in the SAB B2. It should be considered that the construction is located 800–1000 m away from emission sources related to the city's food and metallurgical industry and the vehicular flow related to mass public transportation routes.

Sample B3 is especially rich in Fe (0.0406 ± 0.0035 μg/g/mm^2), V (0.0034 ± 0.0006 μg/g/mm^2) and Cr 0.0015 ± 0.0004 μg/g/mm^2) (Table 4). EDXRF study of the Sr concentration in the external vs internal part of mortars revealed an increment of this element in the external part (90%) versus the internal part (10%) (Table 3). The construction from which SAB B3 sample was extracted host the annual celebration of the carnivals of Barranquilla, in which fireworks shows take place. Unusual levels of Sr and Rb have been reported in fireworks aerosols (these metals together a Ba, Cu, Cr, Ti are used to provide silver and shiny effects) by different authors (Moreno et al., 2007; Hoyos et al., 2020; Pirker et al., 2021; Chatterjee et al., 2013; Schleicher et al., 2012). Therefore, the higher Sr presence in SAB B3 can be associated with this source.

Finally, sample B5 shows the lowest concentrations of metals per mm^2 for all the detected elements. This last agrees with the earliest contruction of the building in comparison with the rest buildings under study. Thefore, in this case, the SABs formed have been exposed less time to the environment, being able to accumulate a lower amount of particulate matter. In spite of that, the concentrations per area of Mn (0.0207 ± 0.0021 μg/g/mm^2 units), Fe (0.1801 ± 0.0023 μg/g/mm^2 units) and Ti (0.0070 ± 0.0005 μg/g/mm^2 units) (Table 4; Figs. 3 and 4; Fig. 7e) are quite high. This last can suggest that the façade of the construction from which this sample has been obtained could be mainly impacted by PM derived from activities related to metal manufacturing processes (for example, galvanizing, crushing, alloy) which are located in that sector of the city. Concretely, Mn could be related to the production of Hadfield steel, which contains Mn at an average concentration of 14–15% (Gasik, 2004).

4. Conclusions

The results presented in this work demonstrate that, in the future, the use of SABs growing of constructions can be explored as a promising

Table 5
Elemental composition of particles studied on SAB samples obtained by EDS as a function of their size.

SAB	Particle type		Elemental composition		
	Single particles (μm)	Cluster particles (μm)	Major (>1%)	Minor (1%–0.1%)	Trace (<0.1%)
B1	5		O, C, Fe, Si	Al, Ca, Cu	Zn, Sn, Pb, Ba, Cr
	10		C, O, Ca, P, Si	Al, Fe, Mg, Rb, Sr, Ni	Zn,
	4		O, C, Ca, Si	Mg	Mn
	5		O, C, Si, Al, K	Cu	V, Pb
		10	O, C, Si, Mg, Al, Fe, Ca	Na, K, Ba	Cr, Sn, Cl, V
		10	O, C, Ca, P, Si	Al, Na, Cu, Fe	Cl, Pb
	2		O, C, Ti, Fe, Si, Ca,	Al	Zn
		20	O, Ti, Fe, Ca, Si, Al	Mg, Mn, K, Ba	Cr, Sb, Pb, V
	4		O, C, N, Ti	Al, Si, Ca, P	Ni, Cu, Cl, K, Pb
		18	O, C, Ca, Si, Al	Fe, Mg, Sr, K, Ti	Zn, Cu, Cr, Mn, Ni, Na, Sn
	15		O, C, Ca, P	Si, Mg, Fe, Na, Al, Br, Sr, Zr, Rb,	Mn, Ti, K, Cr, Ni
	8		C, O	Ca, Si, Al, Mg,	Fe, Rb, Cl
	2		O, Ca, C, Nb, Si	Cu, Ti	
	3		O, C, Ca, Si, Al	Fe, Mg, Sr, K, Ti	P, Sr, Cu, Cr, Mn, Ni, Sn, Na
	2		C, O, Ca, Fe, S, Si	Al	Ni, V
	18		C, Cl, Na, O	Ca, Zn	Pb
	2		O, C, Ti, Fe, Si, Ca, Al	Mn, Zn, V	Ba
		5	O, C, Ca, Si, Al	Fe, Mg, K, Na, Cr, Ba	Mn, Cl, Pb
B2		12	Ni, C, Ca, O, Si, Al	S, Br, Fe, Mg, Na	Mn, Ti, Ba, Cr, Pb
	2		C, O, Si, Ca, Al, S, Fe	Sb	Cu, Cr, Ti
	12		O, Si, Ca, Al, K, Mg	Ti, Na, Fe, Sn, Ni, Sb	Mn, V
	4		O, C, Ca, Ti, Si, Al	Fe, Mg, K, S, Sb	Sn, Ni, Cu
		9	O, Si, Ca, Al, Mg	K, Ti, Fe	Cl
	3		Fe, C, Si	Ca, Cr, Al, Mn, S, Cu, Ni	P, Pb
	6		Fe, C, O, Si	Al, Cr	Na, S, Ni, Ba, Ti
	4		C, O, Ca, Si	Al, K	Cl, Ti
		7	Fe, C, O, Si	Al, Ca, Cr, Mn, Ni	Sb Sn, Rb, Sr
	8		Ba, C, S, O, Ca	Al, Fe, Cr, Mn	Br
	2		C, O, Fe, Ca, Mg, Si	Al, Ni	Mn, V, Zn
	8		C, O, Si, Ca, Mg, Al, K	Br, S	Ni, Ba, Pb, V
	3		C, Fe, O, Si	Cr, Cu	Ba, Pb
		80	C, O, Ca, Si	Al, S, Fe, Ni, K	Mg, Na, Ti, Cl
B3		40	Ba, C, O, S, Ca, Si	Fe	Pb
	4		C, Fe, O, Ca	Si, Mg, S, Sb	Sn, Pb, Ti, Cr
	10		O, C, Mg, Ca, Si, Fe	Al, Cr	V, Sb, Cu
	10		O, Fe, C	Ca, Sb	Mn, Sn, Pb Ba
		5	C, O, Ca, Ni, Br, K	Si, Al, Mg, Sn, Pb	Zn
	6		O, C, S, Ba, Ca	Si, Cr	Pb, Mg, Zn, Rb
		10	Ni, C, O, Ca	Si, Al, Fe	Sb, Pb, Zn, Cu
		12	O, C, Ba, S, Ca	Si, Al, Pb	Zn, Sb
B4		10	Fe, O, C, Cr, Si, Al, Ni	Mn, Ca, Ti, Cu, Rb	Pb, Zn
	2		O, C, Fe, Si, Al, Mg, Ca	Ti, Ba, Mn	V
		3	Fe, Cr, C, Ni, O, Si, Mn	Mg, Ca, Ti	V, Ba
		5	Fe, O, C, Si, Al	Mg, Mn, Rb, Ba	Sr, Pb
		7	O, Si, Al, Fe, Mg	Ca, K, Na, Cr	Sn, Ti, V
	5		Fe, O, Si, Mn, Al, Ca	Na, Ti, Sr, Sb, Ba	Pb
	8		O, Fe, Mn, C, Si	Al, Na, Ca, Ba	Sb
	10		O, Fe, C, Si	Al, Ca, Ti, Ni, Pb	Sr, Rb
B5	2		O, C, Ba, S	Mg, Si, Mn, Fe	Pb, Cr, Zr
	2		O, C, Si, Ca, Ni	Al, Fe, K, Sb	Ti, Cr
	3		O, Ca, Br, K, Si	Sn, Sb	Ti, Cr, Pb
	4		O, C, Ca, Si, Ni	Al, Mg, Fe	V
	25		O, Fe, C, Ca, Si	Mg, Al, Zn	V, Cu, Ti, Cr, Ba
	2		O, C, Ca, Si, Ni, Al	Fe	Ti, V, Pb
		3	O, Ca, Si, Al, S,	Fe, Mg, Cl, Ni, Zn	Pb

alternative to biomonitor atmospheric airborne particulate matter rich in heavy metals. In the future, it would be necessary to carry out additional controlled experiments exposing SABs grown on mortars mock-ups to airborne particulate matter rich in heavy metals. This experiment will allow to quantitatively evaluate the capacity of the SABs to retain the mentioned particles. Apart from the study of the SABs, this work also demonstrates that a selective study of the external and internal (not exposed to the atmosphere) parts of a mortar can offer information about possible accumulations of atmospheric particulate matter in construction materials.

The analytical methology here presented based on the direct use of μ-EDXRF and SEM-EDS single point and imaging strategy has been successfully applied to extract a general overview of the size, nature and distribution of individual and cluster particles deposited on the SABs growing on constructions focusing the attention on the metallic nature of the deposited airborne particulate matter.

Elemental imaging studies of the SABs allowed not only to map the metallic accumulations on them but also to discriminate crusts rich in

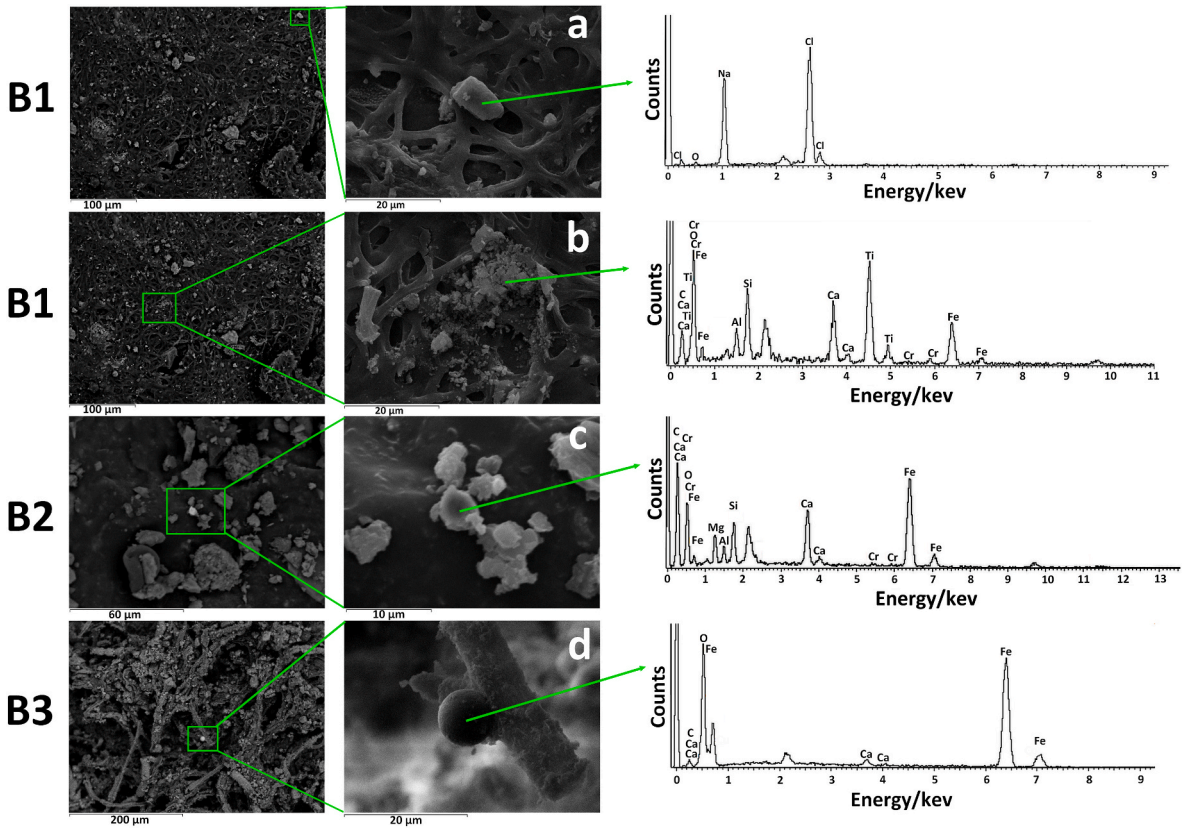

Fig. 5. SEM micrographs of airborne particulate matter deposited on SAB samples B1, B2 and B3 and EDS spectra acquired on the following selected particles: a) 10 μm halite particle deposited on filamentous structures of the biocolonizers of B1. b) 12–18 μm aggregates of titanium oxide and Ca/Fe/Al/Si/Cr deposited on filamentous structures of the biocolonizers of B1. c) 5–7 μm aggregates of aluminosilicate and Fe/Cr deposited on the surface of B2. d) 8 μm aggregates of iron oxide attached to biocolonizer filamentous structure of B3. Note: The non assigned signal in the spectra belongs to Au used to coat the samples.

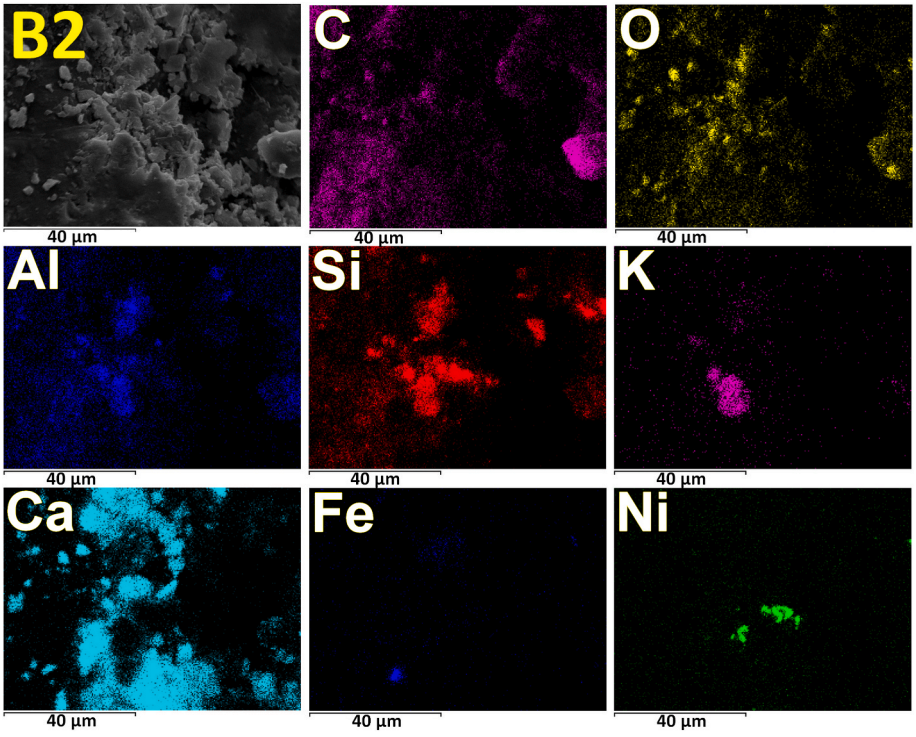

Fig. 6. Elemental distribution maps acquired by SEM–EDS of PM deposited on the SAB B2.

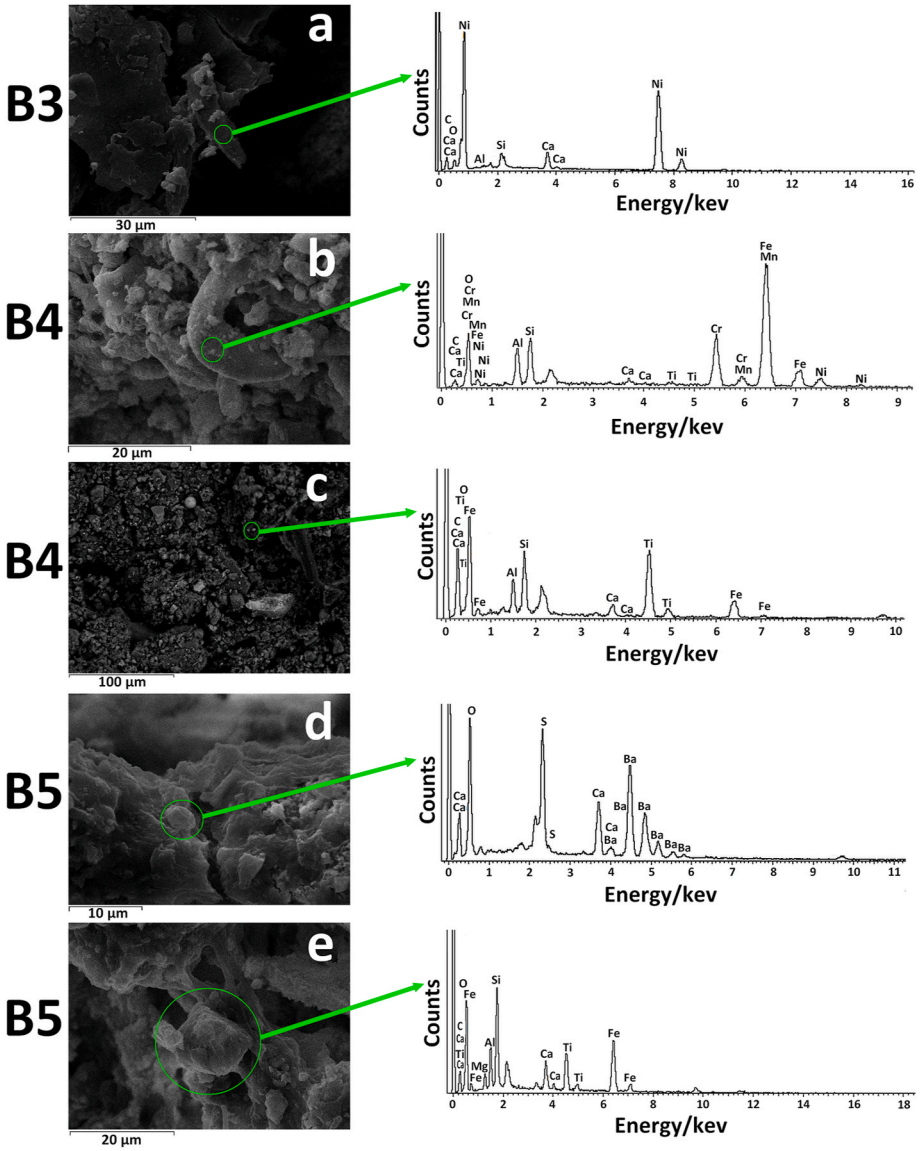

Fig. 7. SEM micrographs of airborne particulate matter deposited on SAB samples B3, B4 and B5 and EDS spectra acquired on the following selected particles. a) 10 μm aggregate of Ni and aluminosilicate deposited on the surface of B3. b) 10–12 μm aggregate iron manganese, aluminosilicate and Ti/Cr/Ni deposited on the surface of B4. c) 5–9 μm μm aggregate of aluminosilicate and Ti/deposited on the surface of B4. d) 3 μm aggregate of barium sulfate and Zn deposited on the surface of B5. e) 10–14 μm aggregates of titanium and iron oxides, aluminosilicate deposited on the surface of B5. Note: The non assigned signal in the spectra belongs to Au used to coat the samples.

heavy metals from real SABs. The semi-quantitative information per unit of area obtained from μ-EDXRF imaging studies of the SABs allowed also to correlate the main metals detected, with nearby anthropogenic impact sources (road traffic, impact of fireworks, impact of metallurgical industry and so on).

SEM-EDS was crucial to perform an in depth study at lower lateral resolution of individual particles or clusters deposited on the SABs. Apart from individual particles of higher dimensions (up to 40 μm), clusters were also identified trapped on the SABs ranging sizes from 20 to 80 μm. In agreement with the μ-EDXRF studies, the predominance of particulate matter rich in Zn, Fe, Mn, Ni and Ti was corroborated by SEM-EDS. This last technique allowed to identify trace metals (down to μg/g), non-detectable by μ-EDXRF imaging such as Ba, Sb, Sn, Cl and Br ($\leq$0,1%).

The obtained results demonstrate the usefulness of this methodology as a relevant tool for environmental monitoring, being a less tedious, time-consuming and environmentally sustainable alternative appropriate to extract quick conclusions helpful to assist stakeholders in environmental health and urban planning. Although this study has been focused in samples of reduced size, considering the availability of transportable macro-XRF scanners able to map bigger surfaces, this methodology can be transferred to bigger façades affected by SABs in order to extract more representative results. This last would help to unequivocally classify SABs spontaneously growing on the façades of constructions as good alternatives to retain particulate matter rich in heavy metals acting as a robust passive sampling alternative.

Author contributions statement

Euler Gallego Cartagena: Conceptualization, Data curation, Formal analysis, Investigation, Methodology, Software, Validation, Visualization, Roles/Writing - original draft, Writing - review & editing, Héctor Morillas: Investigation, Formal analysis, Software, Writing-review & editing. Wendy Morgado-Gamero: Writing - review & editing. Fabio Fuentes-Gandara: Roles/Writing - original draft. Víctor Vacca-Jimeno: Software, Validation. Isabel Salcedo: Visualization. Juan Manuel Madariaga: review & editing. Maite Maguregui: Conceptualization, Data curation, Methodology, Validation, Investigation, Formal analysis, Software, Writing-review & editing.

Declaration of competing interest

The authors declare that they have no known competing financial interests or personal relationships that could have appeared to influence

the work reported in this paper.

Data availability

The authors do not have permission to share data.

Acknowledgments

This work has been supported by the project IT1446-22 for Research Groups of the Basque University System, funded by the Basque Country Government. Open Access funding provided by University of the Basque Country is also gratefully acknowledged. The authors thank for technical and human support provided by SGIker (UPV/EHU/ERDF, EU) and concretely to Alfredo Sarmiento from Coupled Multispectroscopy Singular Laboratory (Raman-LASPEA).

Appendix A. Supplementary data

Supplementary data to this article can be found online at https://doi.org/10.1016/j.chemosphere.2022.136743.

References

Agudelo-Castañeda, D., De Paoli, F., Morgado-Gamero, W., Mendoza, M., Parody, A., Maturana, A., Teixeira, E., 2020. Assessment of the NO_2 distribution and relationship with traffic load in the Caribbean coastal city. Sci. Total Environ. 720, 137675.

Anagnostidis, K., 1986. Modern approach to the classification system of cyanophytes. 2. Chroococcales. Algological Studies/Archiv für Hydrobiologie, Supplement 73, 157–226.

Anagnostidis, K., Komárek, J.A., 1988. A modern approach to the classification systems of cyanophytes 3—Oscillatorales. Arch. Hydrobiol. Suppl. 80, 327–472.

Andrade-Guel, M., Cabello-Alvarado, C., Avila-Orta, C.A., Pérez-Alvarez, M., Cadenas-Pliego, G., Reyes-Rodríguez, P.Y., Ríos-González, L., 2022. Green flame-retardant composites based on PP/TiO_2/lignin obtained by melt-mixing extrusion. Polymers 14 (7), 1300.

Bartnicki-Garcia, S., 1968. Cell wall chemistry, morphogenesis, and taxonomy of fungi. Annu. Rev. Microbiol. 22 (1), 87–108.

Bloise, A., Fornero, E., Belluso, E., Barrese, E., Rinaudo, C., 2008. Synthesis and characterization of tremolite asbestos fibres. Eur. J. Mineral 20 (20), 1027–1033.

Boquete, M.T., Ares, A., Fernandez, J.A., Aboal, J.R., 2020. Matching times: trying to improve the correlation between heavy metal levels in mosses and bulk deposition. Sci. Total Environ. 715, 136955.

Botle, A., Singhal, R.K., Basu, H., Manisha, V., Masih, J., 2020. Health risk assessment of heavy metals associated with Coarse and Quasi-accumulative airborne particulate matter in Mumbai City situated on the Western Coast of India. Environ. Technol. Innovat. 19, 100857.

Carrero, J.A., Arrizabalaga, I., Bustamante, J., Goienaga, N., Arana, G., Madariaga, J.M., 2013. Diagnosing the traffic impact on roadside soils through a multianalytical data analysis of the concentration profiles of traffic-related elements. Sci. Total Environ. 458, 427–434.

Carrero, J.A., Arana, G., Madariaga, J.M., 2014. Use of Raman spectroscopy and scanning electron microscopy for the detection and analysis of road transport pollution. Spectrosc. Prop. Inorg. Organomet. C 45, 178–210.

Castaneda-Miranda, A.G., Chaparro, M.A.E., Pacheco-Castro, A., Chaparro, M.A.E., Bohnel, H.N., 2020. Magnetic biomonitoring of atmospheric dust using tree leaves of *Ficus benjamina* in Queretaro (Mexico). Environ. Monit. Assess. 192 (6), 382.

Chakrabortty, S., Paratkar, G.T., 2006. Biomonitoring of trace element air pollution using mosses. Aerosol Air Qual. Res. 6, 247–258.

Chang, M.B., Huang, C.K., Wu, H.T., Lin, J.J., Chang, S.H., 2000. Characteristics of heavy metals on particles with different sizes from municipal solid waste incineration. J. Hazard Mater. 79 (3), 229–239.

Chatterjee, A., Sarkar, C., Adak, A., Mukherjee, U., Ghosh, S.K., Raha, S., 2013. Ambient air quality during Diwali Festival over Kolkata-a mega-city in India. Aerosol Air Qual. Res. 13 (3), 1133–1144.

Cheng, X., Xu, W., Wang, N., Mu, Y., Zhu, J., Luo, J., 2018. Adsorption of Cu^{2+} and mechanism by natural biofilm. Water Sci. Technol. 78 (4), 721–731.

Chiaia-Hernández, A.C., Scheringer, M., Muller, A., Stieger, G., Wachter, D., Keller, A., Pintado-Herrera, M.G., Lara-Martin, P.A., Bucheli, T.D., Hollender, J., 2020. Target and suspect screening analysis reveals persistent emerging organic contaminants in soils and sediments. Sci. Total Environ. 740, 140181.

Combes, A., Franchineau, G., 2019. Fine particle environmental pollution and cardiovascular diseases. Metabolism 100, 153944.

Contardo, T., Vannini, A., Sharma, K., Giordani, P., Loppi, S., 2020. Disentangling sources of trace element air pollution in complex urban areas by lichen biomonitoring. A case study in Milan (Italy). Chemosphere 256, 127155.

Crispim, C.A., Gaylarde, C.C., 2005. Cyanobacteria and biodeterioration of cultural heritage: a review. Microb. Ecol. 49 (1), 1–9.

Crispim, C.A., Gaylarde, P.M., Gaylarde, C.C., 2003. Algal and cyanobacterial biofilms on calcareous historic buildings. Curr. Microbiol. 46 (2), 79–82.

Cutler, N., Viles, H., 2010. Eukaryotic microorganisms and stone biodeterioration. Geomicrobiol. J. 27, 630–646.

Di Turo, F., Proietti, C., Screpanti, A., Fornasier, M.F., Cionni, I., Favero, G., De Marco, A., 2016. Impacts of air pollution on cultural heritage corrosion at European level: what has been achieved and what are the future scenarios. Environ. Pollut. 218, 586–594.

Gallego-Cartagena, E., Morillas, H., Maguregui, M., Patiño-Camelo, K., Marcaida, I., Morgado-Gamero, W., Silva, L.F.O., Madariaga, J.M., 2020. A comprehensive study of biofilms growing on the built heritage of a Caribbean industrial city in correlation with construction materials. Int. Biodeterior. Biodegrad. 147, 104874.

Gallego-Cartagena, E., Morillas, H., Carrero, J.A., Madariaga, J.M., Maguregui, M., 2021. Naturally growing grimmiaceae family mosses as passive biomonitors of heavy metals pollution in urban-industrial atmospheres from the Bilbao Metropolitan area. Chemosphere 263, 128190.

García-Florentino, C., Maguregui, M., Morillas, H., Marcaida, I., Salcedo, I., Madariaga, J.M., 2018a. *Trentepohlia* algae biofilms as bioindicator of atmospheric metal pollution. Sci. Total Environ. 626, 441–450.

García-Florentino, C., Maguregui, M., Marguí, E., Torrent, L., Queralt, I., Madariaga, J. M., 2018b. Development of Total Reflection X-ray fluorescence spectrometry quantitative methodologies for elemental characterization of building materials and their degradation products. Spectrochim. Acta, Part B 143, 18–25.

García-Florentino, C., Maguregui, M., Ciantelli, C., Sardella, A., Bonazza, A., Queralt, I., Carrero, J.A., Natalí, C., Morillas, H., Madariaga, J.M., Arana, G., 2020. Deciphering past and present atmospheric metal pollution of urban environments: the role of black crusts formed on historical constructions. J. Clean. Prod. 243, 118594.

Gasik, M.I., 2004. Hadfield steel. State-of-the-art of technology and materials science of railway switch frogs. Adv. Electrometall. 1, 27–37.

Gaylarde, C., 2020. Influence of environment on microbial colonization of historic stone buildings with emphasis on cyanobacteria. Heritage 3 (4), 1469–1482.

Gaylarde, C.C., Gaylarde, P.M., 2002. Biodeterioration of historic buildings in Latin America. In: Burn, S. (Ed.), Proceedings of the 9th International Conference on Durability of Materials and Components. Brisbane, Australia.

Glencross, D.A., Ho, T.-R., Camiña, N., Hawrylowicz, C.M., Pfeffer, P.E., 2020. Air pollution and its effects on the immune system. Free Radic. Biol. Med. 151, 56–68.

Grossi, C.M., Brimblecombe, P., 2002. The effect of atmospheric pollution on building materials. J. Phys IV France. 12, 197–210.

Gulotta, D., Villa, F., Cappitelli, F., Toniolo, L., 2018. Biofilm colonization of metamorphic lithotypes of a renaissance cathedral exposed to urban atmosphere. Sci. Total Environ. 639, 1480–1490.

Haikerwal, A., Reisen, F., Sim, M.R., Abramson, M.J., Meyer, C.P., Johnston, F.H., Dennekamp, M., 2015. Impact of smoke from prescribed burning: is it a public health concern? J. Air Waste Manag. 6 (5), 592–598.

Häubner, N., Schumann, R., Karsten, U., 2006. Aeroterrestrial microalgae growing in biofilms on facades—response to temperature and water stress. Microb. Ecol. 51 (3), 285–293.

Hoyos, C.D., Herrera-Mejía, L., Roldán-Henao, N., Isaza, A., 2020. Effects of fireworks on particulate matter concentration in a narrow valley: the case of the Medellín metropolitan area. Environ. Monit. Assess. 192 (1), 1–31.

IDEAM, 2017. «Atlas climatológico de Colombia» 1997. Geografía Física de Barranquilla. Blanco, José A. En: historia General de Barranquilla. In: Mejoras, Primera Edición. Barranquilla, Colombia, ISBN 958-96185-0-2, pp. 13–22.

Islam, N., Saikia, B.K., 2020. Atmospheric particulate matter and potentially hazardous compounds around residential/road side soil in an urban area. Chemosphere 259, 127453.

Karri, V., Schuhmacher, M., Kumar, V., 2016. Heavy metals (Pb, Cd, as and MeHg) as risk factors for cognitive dysfunction: a general review of metal mixture mechanism in brain. Environ. Toxicol. Pharmacol. 48, 203–213.

Kidd, S., Halliday, C., Alexiou, H., Ellis, D., 2016. Descriptions of Medical Fungi, 3^a edition. Adelaide, Australia.

Kurniawan, A., Fukuda, Y., 2022. Analysis of the electric charge properties of biofilm for the development of biofilm matrices as biosorbents for water pollutant. Energ. Ecol. Environ. 1–7.

Lelieveld, J., Evans, J.S., Fnais, M., Giannadaki, D., Pozzer, A., 2015. The contribution of outdoor air pollution sources to premature mortality on a global scale. Nature 525, 367–371.

Lembre, P., Lorentz, C., Di Martino, P., 2012. Exopolysaccharides of the biofilm matrix: a complex biophysical world. In: Karunaratne, D.N. (Ed.), The Complex World of Polysaccharides. InTech Prepress. Rijeka, Croatia, pp. 371–392 (Chapter 13).

Lin, V.S., 2015. Research highlights: natural passive samplers–plants as biomonitors. Environ. Sci.: Process. Impacts 17 (6), 1137–1140.

Liu, E., Yan, T., Birch, G., Zhu, Y., 2014. Pollution and health risk of potentially toxic metals in urban road dust in Nanjing, a mega-city of China. Sci. Total Environ. 476, 522–531.

Liu, F., Zhang, G., Lian, X., Fu, Y., Lin, Q., Yang, Y., Sheng, G., 2022. Influence of meteorological parameters and oxidizing capacity on characteristics of airborne particulate amines in an urban area of the Pearl River Delta, China. Environ. Res. 212, 113212.

López-Bautista, J.M., Rindi, F., Casamatta, D., 2007. The systematics of subaerial algae. In: Seckbach, J. (Ed.), Algae and Cyanobacteria in Extreme Environments. Cellular Origin, Life in Extreme Habitats and Astrobiology, vol. 11. Springer, Dordrecht, pp. 601–617.

Machado, A., García, N., García, C., Acosta, L., Córdova, A., Linares, M., Velásquez, H., 2008. Contaminación por metales (Pb, Zn, Ni y Cr) en aire, sedimentos viales y suelo en una zona de alto tráfico vehicular. Rev. Int. Contam. Ambient. 24 (4), 171–182.

Mariani, R.L., de Mello, W.Z., 2007. $PM_{2.5-10}$, $PM_{2.5}$ and associated water-soluble inorganic species at a coastal urban site in the metropolitan region of Rio de Janeiro. Atmos. Environ. 41 (13), 2887–2892.
Martínez-Arkarazo, I., Angulo, M., Bartolomé, L., Etxebarria, N., Olazabal, M.A., Madariaga, J.M., 2007. An integrated analytical approach to diagnose the conservation state of building materials of a palace house in the metropolitan Bilbao (Basque Country, North of Spain). Anal. Chim. Acta 584 (2), 350–359.
Mitsos, D., Kantarelou, V., Palamara, E., Karydas, A.G., Zacharias, N., Gerasopoulos, E., 2022. Characterization of black crust on archaeological marble from the Library of Hadrian in Athens and inferences about contributing pollution sources. J. Cult. Herit. 53, 236–243.
Moreno, T., Querol, X., Alastuey, A., Minguillón, M.C., Pey, J., Rodriguez, S., Gibbons, W., 2007. Recreational atmospheric pollution episodes: inhalable metalliferous particles from firework displays. Atmos. Environ. 41 (5), 913–922.
Morillas, H., Maguregui, M., García-Florentino, C., Carrero, J.A., Salcedo, I., Madariaga, J.M., 2016. The cauliflower-like black crusts on sandstones: a natural passive sampler to evaluate the surrounding environmental pollution. Environ. Res. 147, 218–232.
Nolte, C., 2016. Identifying challenges to enforcement in protected areas: empirical insights from 15 Colombian parks. Oryx 50 (2), 317–322.
Ogunkunle, C.O., Ziyath, A.M., Rufai, S.S., Fatoba, P.O., 2016. Surrogate approach to determine heavy metal loads in a moss species -*Barbula lambaranensis*-. J. King Saud Univ. Sci. 28, 193–197.
Osorio-Martinez, J., Silva, L.F., Flores, E.M., Nascimento, M.S., Picoloto, R.S., Olivero-Verbel, J., 2021. Environmental and human health risks associated with exposure to hazardous elements present in urban dust from Barranquilla, Colombian Caribbean. J. Environ. Qual. 50 (2), 350–363.
Paglietti, F., Malinconico, S., Conestabile della Staffa, B., Bellagamba, S., De Simone, P., 2016. Classification and management of asbestos-containing waste: European legislation and the Italian experience. Waste Manag. 50, 130–115.
Pant, P., Harrison, R.M., 2013. Estimation of the contribution of road traffic emissions to particulate matter concentrations from field measurements: a review. Atmos. Environ. 77, 78–97.
Paull, N.J., Krix, D., Irga, P.J., Torpy, F.R., 2020. Airborne particulate matter accumulation on common green wall plants. Int. J. Phytoremediation 22 (6), 594–606.
Pinto, A.C., Palomar, T., Alves, L.C., da Silva, S.H.M., Monteiro, R.C., Macedo, M.F., Vilarigues, M.G., 2019. Fungal biodeterioration of stained-glass windows in monuments from Belém do Pará (Brazil). Int. Biodeterior. Biodegrad. 138, 106–113.
Pirker, L., Velkavrh, Ž., Osīte, A., Drinovec, L., Močnik, G., Remškar, M., 2021. Fireworks—a source of nanoparticles, $PM_{2.5}$, PM_{10}, and carbonaceous aerosols. Air. Qual. Atmos. Health 1275–1286.
Poulakis, E., Theodosi, C., Bressi, M., Sciare, J., Ghersi, V., Mihalopoulos, N., 2015. Airborne mineral components and trace metals in Paris region: spatial and temporal variability. Environ. Sci. Pollut. Res. 22 (19), 14663–14672.
Prescott, G.W., 1964. How to know the freshwater algae?. In: How to Know the Freshwater Algae. Michigan State Univ., East Lansing. Wm C. . Brown Company Publishers, Dubuque, Iowa, p. 272.
Prieto-Taboada, N., Ibarrondo, I., Gómez-Laserna, O., Martinez-Arkarazo, I., Olazabal, M. A., Madariaga, J.M., 2013. Buildings as repositories of hazardous pollutants of anthropogenic origin. J. Hazard Mater. 248, 451–460.
Querol, X., Viana, M., Alastuey, A., Amato, F., Moreno, T., Castillo, S., Salvador, P., 2007. Source origin of trace elements in PM from regional background, urban and industrial sites of Spain. Atmos. Environ. 41, 7219–7231.
Radić, M., Brković Dodig, M., Auer, T., 2019. Green facades and living walls —a review establishing the classification of construction types and mapping the benefits. Sustainability 11 (17), 4579.
Ramírez, M., Hernández-Marine, M., Novelo, E., Roldán, M., 2010. Cyanobacteria-containing biofilms from a mayan monument in palenque, Mexico. Biofouling 26 (4), 399–409.
Ramírez-Cerpa, E., Acosta-Coll, M., Vélez-Zapata, J., 2017. Análisis de condiciones climatológicas de precipitaciones de corto plazo en zonas urbanas: caso de estudio Barranquilla, Colombia. IDESIA 35 (2), 87–94.
Rossi, F., De Philippis, R., 2015. Role of cyanobacterial exopolysaccharides in phototrophic biofilms and in complex microbial mats. Life 5 (2), 1218–1238.
Roy, A., Bhattacharya, T., Kumari, M., 2020. Air pollution tolerance, metal accumulation and dust capturing capacity of common tropical trees in commercial and industrial sites. Sci. Total Environ. 722, 137622.
Rubio, M.A., Lissi, E., Riveros, V., Páez, M.A., 2001. Remoción de contaminantes por lluvias y rocíos en la región metropolitana. Bol Soc Chilena Quím. 46 (3), 353–361.
Ruffolo, S.A., Comite, V., La Russa, M.F., Belfiore, C.M., Barca, D., Bonazza, A., Sabbioni, C., 2015. An analysis of the black crusts from the Seville Cathedral: a challenge to deepen the understanding of the relationships among microstructure, microchemical features and pollution sources. Sci. Total Environ. 502, 157–166.
Saiz-Jimenez, C., 1993. Deposition of airborne organic pollutants on historic buildings. Atmos. Environ. B, Urban Atmos. 27 (1), 77–85.
Salo, H., Bućko, M.S., Vaahtovuo, E., Limo, J., Mäkinen, J., Pesonen, L.J., 2012. Biomonitoring of air pollution in SW Finland by magnetic and chemical measurements of moss bags and lichens. J. Geochem. Explor. 115, 69–81.
Scheerer, S., Ortega-Morales, O., Gaylarde, C., 2009. Microbial deterioration of stone monuments-an updated overview. Adv. Appl. Microbiol. 66, 97–139.
Schleicher, N., Norra, S., Chen, Y., Chai, F., Wang, S., 2012. Efficiency of mitigation measures to reduce particulate air pollution—a case study during the Olympic Summer Games 2008 in Beijing, China. Sci. Total Environ. 427, 146–158.
Schraufnagel, D.E., Balmes, J.R., Cowl, C.T., De Matteis, S., Jung, S.H., Mortimer, K., Perez-Padilla, R., Rice, M.B., Riojas-Rodriguez, H., Sood, A., Thurston, G.D., To, T., Vanker, A., Wuebbles, D.J., 2019. Air pollution and noncommunicable diseases: a review by the forum of international respiratory societies' environmental committee, Part 1: the damaging effects of air pollution. Chest 155 (2), 409–416.
Sesana, E., Gagnon, A.S., Bertolin, C., Hughes, J., 2018. Adapting cultural heritage to climate change risks: perspectives of cultural heritage experts in Europe. Geosciences 8 (8), 305.
Srbinovska, M., Andova, V., Mateska, A.K., Krstevska, M.C., 2021. The effect of small green walls on reduction of particulate matter concentration in open areas. J. Clean. Prod. 279, 123306.
Sun, F., Yun, D.A.I., Yu, X., 2017. Air pollution, food production and food security: a review from the perspective of food system. J. Integr. Agric. 16 (12), 2945–2962.
Sun, Y., Lu, Y., Saredy, J., Wang, X., Drummer IV, C., Shao, Y., Saaoud, F., Xu, K., Liu, M., Yang, W.Y., Jiang, X., Wang, H., Yang, X., 2020. ROS systems are a new integrated network for sensing homeostasis and alarming stresses in organelle metabolic processes. Redox Biol. 37, 101696.
Szynkowska, M.I., Pawlaczyk, A., Mackiewicz, E., 2018. Bioaccumulation and biomagnification of trace elements in the environment. In: Chojnacka, K., Saeid, A. (Eds.), Recent Advances in Trace Elements. Wroclaw, Poland, pp. 249–251 (Chapter 13).
Tchounwou, P.B., Yedjou, C.G., Patlolla, A.K., Sutton, D.J., 2012. Heavy metal toxicity and the environment. In: Luch, A. (Ed.), Molecular, Clinical and Environmental Toxicology. Experientia Supplementum, vol. 101. Springer, Basel.
Vianna, N.A., Gonçalves, D., Brandão, F., de Barros, R.P., Meire, R.O., Torres, J.P.M., Andrade, L.R., 2011. Assessment of heavy metals in the particulate matter of two Brazilian metropolitan areas by using *Tillandsia usneoides* as atmospheric biomonitor. Environ. Sci. Pollut. Res. 18 (3), 416–427.
Villa, F., Cappitelli, F., 2019. The ecology of subaerial biofilms in dry and inhospitable terrestrial environments. Microorganisms 7 (10), 380.
Villa, F., Pitts, B., Lauchnor, E., Cappitelli, F., Stewart, P.S., 2015. Development of a laboratory model of a phototroph-heterotroph mixed-species biofilm at the stone/air interface. Front. Microbiol. 6, 1251.
Villa, F., Stewart, P.S., Klapper, I., Jacob, J.M., Cappitelli, F., 2016. Subaerial biofilms on outdoor stone monuments: changing the perspective toward an ecological framework. Bioscience 66 (4), 285–294.
Vojtková, H., 2017. Algae and their biodegradation effects on building materials in the Ostrava industrial agglomeration. In: Proceedings of the 1st International Conference on Advances in Environmental Engineering (AEE), vol. 92. Czech Republic, Ostrava, pp. 28–30.
Wang, Z., Li, J., Mu, X., Zhao, L., Gu, C., Gao, H., Huang, T., 2021. A WRF-CMAQ modeling of atmospheric PAH cycling and health risks in the heavy petrochemical industrialized Lanzhou valley, Northwest China. J. Clean. Prod. 291, 125989.
Wannaz, E.D., Abril, G.A., Rodriguez, J.H., Pignata, M.L., 2013. Assessment of polycyclic aromatic hydrocarbons in industrial and urban areas using passive air samplers and leaves of *Tillandsia capillaris*. J. Environ. Chem. Eng. 1, 1028–1035.
Weber, R.W., Pitt, D., 2000. Teaching techniques for mycology: 11. Riddell's slide cultures. Mycologist 14 (3), 118–120.
World Health Organization, 2016. Exposure to ambient air pollution, Chapter 2. In: Ambient Air Pollution: a Global Assessment of Exposure and Burden of Disease. World Health Organization. Inis Communication, Geneva, Switzerland, pp. 23–28.
Zafra, C., Temprano, J., Tejero, I.A., 2016. The physical factors affecting heavy metals accumulated in the sediment deposited on road surfaces in dry weather: a review. Urban Water J. 14, 639–649.
Zerboni, A., Villa, F., Wu, Y.L., Solomon, T., Trentini, A., Rizzi, A., Gallinaro, M., 2022. The sustainability of rock art: preservation and Research. Sustainability 14 (10), 6305.
Zhang, K., Batterman, S., 2013. Air pollution and health risks due to vehicle traffic. Sci. Total Environ. 450, 307–316.
Zhang, K., Chai, F., Zheng, Z., Yang, Q., Zhong, X., Fomba, K.W., Zhou, G., 2018. Size distribution and source of heavy metals in particulate matter on the lead and zinc smelting affected area. J. Environ. Sci. 71, 188–196.
Zhou, S., Cong, L., Liu, J., Zhang, Z., 2022. Consistency between deposition of particulate matter and its removal by rainfall from leaf surfaces in plant canopies. Ecotoxicol. Environ. Saf. 240, 113679.